Draft version July 4, 2014
Preprint typeset using LaTeX style emulateapj v. 11/12/01

arXiv:1407.0845v1 [astro-ph.HE] 3 Jul 2014

EVIDENCE OF THERMONUCLEAR FLAME SPREADING ON NEUTRON STARS FROM BURST RISE OSCILLATIONS

Manoneeta Chakraborty[1] and Sudip Bhattacharyya[1]
Draft version July 4, 2014

ABSTRACT

Burst oscillations during the rising phases of thermonuclear X-ray bursts are usually believed to originate from flame spreading on the neutron star surface. However, the decrease of fractional oscillation amplitude with rise time, which provides a main observational support for the flame spreading model, have so far been reported from only a few bursts. Moreover, the non-detection and intermittent detections of rise oscillations from many bursts are not yet understood considering the flame spreading scenario. Here, we report the decreasing trend of fractional oscillation amplitude from an extensive analysis of a large sample of *Rossi X-ray Timing Explorer* Proportional Counter Array bursts from ten neutron star low-mass X-ray binaries. This trend is 99.99% significant for the best case, which provides, to the best of our knowledge, by far the strongest evidence of such trend. Moreover, it is important to note that an opposite trend is not found from any of the bursts. The concave shape of the fractional amplitude profiles for all the bursts suggests latitude-dependent flame speeds, possibly due to the effects of the Coriolis force. We also systematically study the roles of low fractional amplitude and low count rate for non-detection and intermittent detections of rise oscillations, and attempt to understand them within the flame spreading scenario. Our results support a weak turbulent viscosity for flame spreading, and imply that burst rise oscillations originate from an expanding hot spot, thus making these oscillations a more reliable tool to constrain the neutron star equations of state.

Subject headings: accretion, accretion disks — equation of state — methods: data analysis — stars: neutron — X-rays: binaries — X-rays: bursts

1. INTRODUCTION

Thermonuclear or type I X-ray bursts are eruptions in X-rays, observed from many neutron star low-mass X-ray binary (LMXB) systems (Strohmayer & Bildsten 2006; Galloway et al. 2008). Intermittent unstable burning of the accreted matter accumulated on the neutron star surface causes these bursts (Lamb & Lamb 1978; Swank et al. 1977). During such a burst, the observed X-ray intensity increases by a factor of ~ 10 in $\approx 0.5-5$ s, and then decays in $\approx 10-100$ s as the stellar surface cools down. These bursts may belong to various burning regimes based on the chemical composition of the fuel and the accretion rate per unit stellar surface area. For example, a burst may be a mixed hydrogen and helium burst triggered by hydrogen ignition, or a pure helium burst, or a mixed hydrogen and helium burst triggered by helium ignition (Strohmayer & Bildsten (2006) and references therein). The spectral and timing properties of these bursts can be a useful tool to measure neutron star parameters, and hence to constrain the equation of state (EoS) models of super-dense degenerate matter of stellar cores (Bhattacharyya (2010) and references therein).

Some bursts from several neutron star LMXBs show X-ray intensity fluctuations, termed as burst oscillations (Watts (2012) and references therein). They originate from the azimuthally asymmetric brightness pattern on the surface of a spinning neutron star (Chakrabarty et al. 2003; Strohmayer et al. 2003). This feature can appear during the rise and/or the decay of the burst. The frequency of these oscillations is close (better than $\approx 1\%$) to the stellar spin frequency, and can evolve by a value between a fraction of a Hz to a few Hz during a burst (Watts (2012) and references therein). Burst oscillations are used to measure neutron star spin rates (e.g., Bhattacharyya (2007); Chakraborty & Bhattacharyya (2012); Watts (2012)). Moreover, the phase-folded light curves of burst oscillations can be fitted with appropriate relativistic models to constrain other stellar parameters, such as mass and radius (Bhattacharyya 2010; Miller & Lamb 1998; Nath et al. 2002; Bhattacharyya et al. 2005; Lo et al. 2013). However, in order to use this method reliably, it will be helpful to understand the origin and nature of the asymmetric brightness pattern on the stellar surface.

In this paper, we focus on the oscillations during burst rise. Such rise oscillations could originate from an expanding hotspot or burning region (Watts 2012). This is because ignition is expected to happen at a certain point on the neutron star surface, and then the thermonuclear flames should spread to ignite all the fuel (Fryxell & Woosley 1982; Cumming & Bildsten 2000).

Thermonuclear flames should spread by deflagration on neutron stars (Spitkovsky et al. 2002). These authors studied flame spreading on rapidly spinning neutron stars considering the effects of the Coriolis force and the lift-up of the burning ocean. Their calculations show that the flame spreads rapidly by geostrophic flow initially after ignition. A typical speed of this geostrohic flow can be $\vartheta_{geostrophic} \approx (gh)^{1/2} \sim 4.5 \times 10^3$ km s^{-1}, where g is the gravitational acceleration and h is the scale height of the burning region (Spitkovsky et al. 2002). But when the burning region becomes sufficiently large making the Rossby number less than 1, the Coriolis force comes

[1] Department of Astronomy and Astrophysics, Tata Institute of Fundamental Research, 1 Homi Bhabha Road, Mumbai 400005, India; manoneeta@tifr.res.in; sudip@tifr.res.in

into play, and slows down the burning front. The flame then spreads by much slower ageostrophic speed. For a weak turbulent viscosity, this ageostrophic flame speed is $\vartheta_{\rm flame} \sim (gh)^{1/2}/ft_{\rm n} \sim 5-20$ km s^{-1}. Here, $t_{\rm n}$ is the time scale of nuclear burning, and the Coriolis parameter $f = 2\Omega\sin\theta$, where Ω is the stellar angular speed and θ is the latitude of the burning front. For a dynamically important turbulent viscosity, the ageostrophic flame speed is maximum: $\vartheta_{\rm flame} \sim (gh/ft_{\rm n})^{1/2} \sim 100-300$ km s^{-1}. Therefore, an observational estimate of the time-scale of flame spreading can be useful to probe the viscosity and g, h and $t_{\rm n}$ (note that Ω is known from burst oscillations). After Spitkovsky et al. (2002), a recent work (Cavecchi et al. 2013) has reported vertically resolved hydrodynamic simulations of flame spreading via deflagration in the thin helium ocean of a spinning star. But this paper assumes a constant Coriolis parameter, and hence does not study the latitude dependence of flame speed.

Observational indications of thermonuclear flame spreading have been found from decreasing fractional amplitude of burst rise oscillations (Strohmayer et al. 1997, 1998; van Straaten et al. 2001; Nath et al. 2002; Bhattacharyya & Strohmayer 2005, 2006c). This is because, as the burning region expands on a spinning neutron star, an increasingly larger fraction of this region usually remains visible throughout the spin period. However, to the best of our knowledge, the decreasing trend has not been quantified by fitting with empirical models and by doing F-tests.

The evolution of fractional amplitude during burst rise can not only be useful to probe thermonuclear flame spreading, but also to detect the effects of the Coriolis force on such spreading. This is because, as Bhattacharyya & Strohmayer (2007b) showed by numerical calculations, a convex-shaped fractional amplitude profile implies isotropic flame speeds and a concave-shaped fractional amplitude profile implies latitude-dependent flame speeds, possibly influenced by the Coriolis force. Bhattacharyya & Strohmayer (2005, 2006c, 2007b) showed two examples of apparently concave-shaped profiles for two bursts, but these authors or any other authors did not quantify the shapes of fractional amplitude profiles of burst rise oscillations in an attempt to detect latitude-dependent flame speeds. Apart from fractional amplitude profiles, indications of flame spreading were also found from weak double-peaked bursts (Bhattacharyya & Strohmayer 2006a,b), as well as from an unusual precursor burst with oscillations (Bhattacharyya & Strohmayer 2007a). Finally, Maurer & Watts (2008) divided the bursts into three groups based on their peak fluxes and 'rise light curve morphology', and connected these groups to various burning regimes, ignition latitudes and flame spreading parameters.

In spite of some observational indications of thermonuclear flame spreading during burst rise, several issues exist. The first one is why oscillations are not detected during the rise of most bursts. Is it because (1) the count rate is too low; or (2) flames spread too fast, so that the spreading is over at the beginning of the rise when the intensity is low; or (3) the ignition happens at a latitude which is not visible due to the viewing angle of the observer, and then, when the burning region can be seen, it becomes azimuthally symmetric; or (4) the visible portion of the burning region is azimuthally symmetric almost from the beginning? One needs to answer this question to know whether burst rise oscillations originate from flame spreading. Therefore, a more systematic and extensive study is required to check if the available burst rise data, including the upper limits, are consistent with the expanding burning region model (Watts 2012).

In this paper, we systematically analyze the *Rossi X-ray Timing Explorer* (*RXTE*) Proportional Counter Array (PCA) data of 51 thermonuclear bursts from ten neutron star LMXBs. We primarily focus on the bursts from the prolific burster 4U 1636–536, harboring a rapidly spinning (frequency ≈ 582 Hz; Strohmayer & Markwardt (2002)) neutron star. We find that the non-detection of oscillations during the rise of most bursts from 4U 1636–536 is not solely due to the low count rates. We extensively examine the fractional amplitude evolution during the rising phase of all the 51 bursts, and show that such evolution is consistent with rise oscillations originating from flame spreading, possibly influenced by the Coriolis force. We explain our methods in § 2, describe the results with figures in § 3, discuss the implications of the results in § 4, and summarize the key points of the paper in § 5.

2. DATA ANALYSIS

2.1. *Data description*

We choose the *RXTE* PCA bursts for our analysis in the following way. We use only the data from the Galloway et al. (2008) catalogue, because (1) *RXTE* usually operated with only one or two proportional counter units (PCUs) on in the recent years, and hence the later data generally had poorer statistics, and (2) Galloway et al. (2008) give a good representative sample of bursts. In this catalogue, 12 sources with burst rise oscillations are mentioned, out of which two are pulsars. We exclude pulsars from our analysis, because the periodic pulsations and the burst oscillations are difficult to distinguish. The rest ten sources are 4U 1636–536, 4U 1608–52, MXB 1659–298, 4U 1702–429, 4U 1728–34, KS 1731–260, 1A 1744–361, SAX J1750.8–2900, 4U 1916–053 and Aql X–1. Neutron stars in all these sources are rapidly spinning (see Tables 1 and 2). Galloway et al. (2008) reported rise oscillations from 32 bursts out of 172 PCA bursts from 4U 1636–536, and rise oscillations from 41 bursts out of 315 PCA bursts from the other nine sources. We use the bursts from all the ten sources to study the evolution of fractional amplitudes of rise oscillations (§ 3.2 and 3.3). In order to probe the cause of non-detection and intermittent detection of burst rise oscillations from many bursts (§ 3.1), as well as to study the burst properties in various bursts groups (§ 3.4), we use the bursts only from 4U 1636–536. This is because this source showed by far the highest number of bursts with rise oscillations (see Tables 1 and 2). We consider 161 out of 172 bursts for 4U 1636–536, because the rising phases of the rest of the bursts were at most partially observed. Finally, we note that the analysis of event mode data (time resolution ≈ 122 μs) from *RXTE* PCA is reported in this paper (Jahoda et al. 2006).

2.2. *Fractional amplitude calculation*

A primary aim of this work is to study the fractional amplitude evolution of burst rise oscillations observed from neutron star LMXBs. To begin with, we define the rise time of each burst as the time in which the pre-burst level subtracted PCA count rate increases from the 5% of the peak to the peak. Then we divide the rise time of every burst into 0.25 s bins for the sake of a systematic and uniform analysis. Such a small time bin is necessary to track the burst oscillation amplitude evolution, especially just after the burst onset, when the amplitude possibly evolves fast (Bhattacharyya & Strohmayer 2007b). Moreover, equal time bins are required to use a uniform detection criterion and to study the non-detection and intermittent detections of burst rise oscillations from many bursts, as discussed later. After dividing the rise time into bins, we check whether burst oscillation is detected in a time bin, and estimate the fractional amplitude for that bin.

A time bin size of 0.25 s implies a very coarse frequency resolution of 4 Hz, when the light curve is Fourier transformed. Consequently, a conventional method of static power spectrum cannot be used either to estimate the fractional amplitude, or to estimate the frequency of oscillations for a time bin. Therefore, a phase-timing analysis is usually used to estimate the frequency evolution (Muno et al. 2000; Strohmayer & Markwardt 2002; Bhattacharyya & Strohmayer 2006c). Then the resulting best-fit frequency versus time profile is used to calculate the fractional amplitude for each time bin using the phase-folded light curve (see below). The results of this phase-timing analysis very well match with those of an alternative technique of Z^2 power maximization for the entire rise interval (Strohmayer & Markwardt 2002; Bhattacharyya & Strohmayer 2006c). However, the frequency model should have a small number of free parameters, and the oscillation should be present in several rise time bins, for the phase-timing analysis technique to work well. But frequency appears to change apparently erratically, and oscillation is present only for short intervals during the rise of many bursts (Fig. 1 shows an example of such a burst). Therefore, we cannot use the phase-timing analysis technique for many bursts. Consequently, we use an alternative method to estimate the frequency−time profile, as we aim for a uniform analysis for all the bursts.

Here we describe this method. We adopt the following procedure to estimate the oscillation frequency. We assume that this frequency remains constant in a time bin, which may usually be justified for a small bin size of 0.25 s. Then we estimate this frequency by maximizing the fractional amplitude using the phase-folded light curves for frequency values in the range (ν_1, ν_2) with a step size of $\Delta\nu$ (e.g., Strohmayer et al. (1998)). Here, $\nu_1 < \nu_{\rm star} < \nu_2$, where $\nu_{\rm star}$ is the known spin frequency of the neutron star. Moreover, we consider $\nu_2 - \nu_1 \sim 5$ Hz, since the burst oscillation frequency of a given source does not change by more than 5 Hz. This fractional amplitude maximization technique is similar to the Z^2 power maximization technique mentioned above. In the next paragraph, we describe how the fractional amplitude is estimated for a given frequency value.

For an oscillation frequency $\nu_{\rm osc}$ for a given time bin, we extract the phase-folded light curve from the event mode data within the 0.25 s bin, after subtracting the persistent intensity level (Bhattacharyya & Strohmayer 2005). The persistent level is calculated averaging 20 s of pre-burst emission, or emission well after the bursts if the pre-burst data are not available. The number of phase bins used is 16 and the error of a bin of the phase-folded light curve is computed by propagating the errors of total emission and persistent emission. Following the standard technique, a phase-folded light curve is fitted with a constant plus a sinusoid: $A + B\sin(2\pi\nu t + \delta)$, where A and B are free parameters and $\nu = \nu_{\rm osc}$ (Bhattacharyya & Strohmayer 2005; Muno et al. 2000). Any additional harmonic content, if present at all, is too weak to detect. We find that a 'constant+sinusoid' model with harmonic is *not* better than a simple 'constant+sinusoid' model with more than 95.45% (i.e, 2σ) significance. This is supported by the fact that the only report of harmonic component in burst rise oscillations from any source was by Bhattacharyya & Strohmayer (2005), who combined the first 1/3rd of the rise time intervals of nine bursts from 4U 1636–536 to detect the harmonic with 3σ. If the oscillation is detected (see the next paragraph) for the chosen time bin, then the fractional root-mean-squared (rms) amplitude for that bin is $r = B/(\sqrt{2}A)$, where the best-fit values of A and B, for the frequency which maximizes the fractional amplitude, are used. The error ($r^{\rm err}$) of r is estimated by propagating the errors of A and B.

Now we describe our procedure to check if the oscillation is detected for the chosen time bin. For this, we fit the phase-folded light curve also with a constant A', and perform an F-test between the constant model and the 'constant+sinusoid' model. If the latter model is at least 3σ more significant than the former one, i.e., if the probability that the 'constant+sinusoid' model is better that the constant model only by random chances is 0.0027 or less, we consider that the burst oscillation is detected. If the oscillation is not detected, we estimate the upper limit of r, which is the maximum value of $r + r^{\rm err}$ for all the values of ν in the range (ν_1, ν_2) with the step size of $\Delta\nu$ (see before in this subsection for the meanings of ν_1, ν_2 and $\Delta\nu$). Galloway et al. (2008) reported the detection of burst rise oscillations for 32 PCA bursts from 4U 1636–536 and for 41 PCA bursts from other nine sources (Table 2; § 2.1). With our above mentioned criterion, we detect rise oscillation for at least one 0.25 s time bin for 27 bursts from 4U 1636–536 (Table 1) and for 24 bursts from other nine sources (Table 2). This is because our detection criterion is quite stringent considering the small numbers of total counts in short 0.25 s time bins. Such stringent criterion contributes to the reliability of our conclusions.

Since we do not use the standard phase-timing analysis technique to estimate the oscillation frequencies, we need to do a sanity check for our results. Therefore, we estimate the fractional rms amplitude profiles using our method and the phase-timing analysis technique for a few bursts. We find that for a given burst, such profiles from two methods are consistent with each other. We show this with an example burst in Fig. 2. Here the fractional rms amplitude values from the two methods differ typically by 4.5% (≈ 0.26 times the 1 σ error from our analysis).

We furthermore note that the non-constant intensity within a 0.25 s burst time bin does not tangibly affect

our fractional rms amplitude value, as we find from detailed simulations. In our simulations, we assume a constant fractional amplitude in a time bin with the steepest count rate slope available from the data. We find that our estimated fractional rms amplitude value is systematically less than the correct value which includes the effect of non-constant intensity, but this systematic error contributes to the total error by less than 0.4% for our typical data count rates.

Now an important question to ask is what determines the detection of burst oscillations. This will be useful to understand why oscillations are not detected during the rise of most bursts (see § 1). The detection of burst oscillation in a time bin depends on the signal to noise ratio (S/N). To represent the S/N, we use the figure of merit quantity

$$\frac{\Delta N}{N^{\rm err}} = \frac{\Delta N}{N_{\rm T}-N_{\rm Per}}\frac{N_{\rm T}-N_{\rm Per}}{N^{\rm err}} = \sqrt{2}r\frac{N_{\rm T}-N_{\rm Per}}{N^{\rm err}}, \quad (1)$$

where, ΔN is the absolute peak amplitude (in count rate) of oscillation, $N_{\rm T}$ is the total count rate averaged over a time bin, $N_{\rm Per}$ is the average persistent count rate, $N^{\rm err}$ is the estimated error on $N_{\rm T}-N_{\rm Per}$, and r is the fractional rms amplitude. Note that ΔN and $N_{\rm T}-N_{\rm Per}$ are essentially B and A respectively, where the latter two are free parameters in the previously mentioned 'constant+sinusoid' model $A+B\sin(2\pi\nu t+\delta)$ of phase-folded oscillation light curves. Eqn. 1 shows that for a given strength (i.e., r) of the burst rise oscillation, the detection of oscillation depends on the count rate parameter $\frac{N_{\rm T}-N_{\rm Per}}{N^{\rm err}}$. Therefore, we calculate this parameter for all the 0.25 s rise time bins of all the 161 bursts (§ 2.1) from 4U 1636–536.

2.3. *Burst rise morphology characterization*

Following Maurer & Watts (2008) (see also § 1), we estimate the shapes of the rise light curves of 27 bursts with oscillations detected during rise (see Table 1). For this morphology analysis, we consider the burst rise as the time interval between 5% and 90% of the peak PCA count rate, after correcting for the persistent emission. In order to make an uniform comparison among different bursts, we normalize both the rise intensity and the rise time of each burst so that they increase from 0 to 10 in dimensionless units. The shape of a burst rise light curve is expressed with a quantity $\mathcal{C}$, which gives a measure of the degree of light curve convexity as

$$\mathcal{C} = \sum_{i=0}^{M}(R_i - x_i)\Delta t, \quad (2)$$

where R_i and x_i are respectively the re-normalized count rate and the re-normalized rise time in each bin, Δt is the re-normalized time bin size, and M is the number of such re-normalized time bins. In the chosen units, $\mathcal{C}$ lies between -50 and 50, and it is positive for an overall convex shape and negative for an overall concave shape.

2.4. *Estimation of persistent emission change*

The recent work of Worpel et al. (2013) suggests a change of persistent emission from its pre-burst value during thermonuclear X-ray bursts. These authors multiplied the best-fit pre-burst emission spectrum with a factor f_a to represent the persistent emission spectrum during a burst. They generally found $f_a \neq 1$, which indicated a change of persistent emission during a burst. Such change would introduce a systematic error in our calculated fractional rms amplitudes, as described in § 2.2. Hence we estimate this persistent emission change (following Worpel et al. (2013)) for each of 27 bursts from 4U 1636–536 with detected rise oscillations (see Table 1), and examine if this change has any significant effect on fractional amplitude evolution.

For spectral analysis we use the same 0.25 s time bins during burst rise (see § 2.2), and extract the energy spectrum from each bin. Each spectrum is fitted within $3-15$ keV in XSPEC using the model `wabs*bbodyrad+constant*`$P(E)$, where `wabs` is an absorption model, `bbodyrad` is a blackbody model, the constant is the multiplicative factor f_a, and $P(E)$ is the fixed persistent emission spectral model `wabs*(bbodyrad+powerlaw)` with best-fit parameters. These best-fit parameters of persistent emission model are estimated from spectral fitting of a 100 s time segment either prior to the burst or well after the burst. The background for this fitting is calculated using the FTOOLS command 'PCABACKEST'. The neutral hydrogen column density ($N_{\rm H}$) parameter in the `wabs` component is frozen at 0.25×10^{22} cm^{-2} (Asai et al. 2000), and a 0.5% systematic error is assumed. For the fitting we have used Churazov weighting to take care of the low count statistics. From the time resolved spectroscopy we obtain the value of f_a and its error for each time bin.

Then the fractional rms amplitude and its error are recalculated, or the upper limit of the amplitude is re-estimated (in case of non-detection) for each 0.25 s time bin using this f_a and its error for each bin. However, given the available quality of data, there are the following difficulties in reliably estimating the fractional amplitude evolution including the effects of f_a. (1) The usually large statistical error of f_a makes the errors on the count rates of the phase-folded light curves larger. This reduces the number of 0.25 s time bins with detection of oscillations, increases the error on fractional amplitudes, and makes the trend of the amplitude evolution less clear. (2) The fitting cannot be performed for some time bins as the statistics is very poor. f_a and its error cannot be calculated for these bins and consequently the modified rms amplitude cannot be determined. This results in some missing data points in the rms amplitude evolution making the trend weaker. For these reasons, we report the fractional amplitudes primarily without considering the change of persistent emission during a burst, and check if the resulting conclusions are consistent with those from the 'f_a method' mentioned in this subsection.

3. RESULTS

3.1. *Detection of oscillations for 4U 1636–536*

In order to understand why burst rise oscillations are not detected from most bursts from 4U 1636–536, we plot the count rate parameter versus 0.25 s time bin index for all 161 bursts in Fig. 3 (see § 2.2 for some details). This figure clearly shows that, for each bin, some bursts with oscillations can have much lower count rate parameter val-

ues than some of those without oscillations. Oscillations during rise are detected in 1 bin for 9 bursts, in 2 bins for 9 bursts, in 3 bins for 5 bursts and in 4, 6, 7 and 9 bins for 1 burst each. In order to further check whether oscillations from more bursts are detected as the intensity (and also the count rate parameter) increases during the rise, we show, for each bin, the ratio of the number of bursts with oscillations to the total number of bursts in Fig. 4. This figure shows that the detected fraction has an overall decreasing trend with time. Therefore, Figs. 3 and 4 imply that the detection of oscillation depends on the fractional amplitude value. Note that, in both Figs. 3 and 4, we consider the first ten 0.25 s time bins (or all the bins if the number is not more than ten for a burst), because the later time bins do not usually have any detected oscillation.

In order to find out if the evolution of persistent emission during a burst changes the above finding, we calculate the count rate parameter values including f_a (see § 2.4). With these modified count rate parameter values, we make a figure (Fig. 5) similar to Fig. 3 for the 27 bursts mentioned in Table 1. We find that, even for the change of persistent emission, the non-detections of burst rise oscillations are not solely due to the low count rates.

However, the burst intensity may also affect the detection of oscillations. In order to check this, we plot the distributions of 0.25 s rise time bins of all the 161 bursts from 4U 1636–536 over the count rate parameter values in the following two cases: (1) bins without detected oscillations, and (2) bins with detected oscillations; both without considering f_a (see Fig. 6). From this figure, it appears that the second distribution is somewhat shifted towards the higher values of the count rate parameter relative to the first distribution. If true, this would imply that the burst intensity affects the detection of oscillations. In order to quantify the difference between the two distributions, we perform a Kolmogorov-Smirnov (K-S) test between them. We obtain a maximum deviation of 0.243 between the two distributions with a significance level of 6.9×10^{-4}, i.e, the probability that the two distributions are same is small (6.9×10^{-4}). This implies that the detection of oscillations depends, not only on the fractional amplitude value as shown earlier, but also on the count rate parameter, and hence on the burst intensity.

3.2. *Fractional amplitude evolution for 4U 1636–536*

We compute the fractional rms amplitude evolution of burst rise oscillations of all the 27 *RXTE* PCA bursts from 4U 1636–536 (mentioned in Table 1). The fractional amplitudes are plotted with time in Fig. 7. This figure indicates that, in spite of the oscillations being usually intermittent and short-lived, the fractional amplitude appears to decrease with time. Moreover, the fractional amplitude evolution seems to have a concave shape, i.e., the amplitude initially decreases fast and then does not change much. In order to verify these, we fit the fractional amplitude curves with an empirical model of the form

$$\phi = a - bc(1 - e^{-t/c}), \tag{3}$$

with the parameters $a > 0$, $b > 0$ and c. This is a convenient function because constraints on a and b ensure that it monotonically decreases with time t. A positive value of c implies a concave fractional rms amplitude versus time curve, while a negative value implies a convex curve.

For two bursts (16 and 18) the rise oscillations are detected for relatively long durations, i.e., in minimum five time bins, including at least one of the first two bins (see Fig. 7). We fit the time evolution of fractional rms amplitude of detected points (excluding the upper limits) with a constant model and the ϕ-model (Eqn. 3) for these bursts. The χ^2/d.o.f. values obtained for the constant and the ϕ-model are 22.5/8 and 1.0/6 respectively for the burst 16, and 19.4/6 and 4.0/4 respectively for the burst 18. Then we perform F-tests between the two models for these two bursts, and find that the ϕ-model is better than the constant model with a significance of $\approx 4\sigma$ and $\approx 2\sigma$ for burst 16 and 18 respectively. Therefore, it may be inferred that the fractional amplitude decreases with time with a significance of $\approx 99.99\%$ and $\approx 95.45\%$ for these two bursts. The best-fit values of the c-parameter are 0.46 ± 0.21 and 0.42 ± 0.19 for burst numbers 16 and 18 respectively, which imply concave-shaped fractional amplitude versus time curves (see Fig 8).

In order to check if the c-parameter is positive when the upper limits are considered for fitting, we fit the fractional amplitude versus time curves, including both the upper limits and the detected points, with the ϕ-model. The best-fit parameter values are obtained by maximizing the likelihood function modified for censored data (i.e, data comprising of upper limits; Feigelson & Nelson (1985); Isobe et al. (1986); Wolynetz (1979a,b)). This method can be effectively employed if the number of detected points is not much lesser than the number of censored points (Isobe et al. 1986). With this constraint, we can apply this technique for modelling the fractional amplitude evolution of seven bursts, and estimate the best-fit parameter values. Examples of the best-fit model curves are shown in panels 5 and 16 of Fig. 7 (green dash-dot curves). The best-fit c-parameter values are plotted in the left panel of Fig. 8. This panel shows that all the seven best-fit c values are positive. Moreover, the best-fit values of c from fits with and without upper limits are consistent with each other for bursts 16 and 18 (left panel of Fig. 8).

Since the above mentioned likelihood maximization technique cannot be applied for all the 27 bursts (Table 1), we fit all the fractional amplitude versus time curves (including upper limits) with the ϕ-model using the weighted least square (a generalized form of χ^2; Feigelson & Babu (2013)) minimization method. The weighted least square L^2 is defined as $\sum \frac{1}{\sigma_i^2}(R_i - R_{mi})^2$, where R_i is the observed fractional rms amplitude, R_{mi} is the model fractional rms amplitude and σ_i is either an assumed error for an upper limit or the measured error for a detected point. For an upper limit, we consider an asymmetric error, with the upper error weighted with a very small factor (to ensure that the model curve usually remains below the upper limit) and the lower error weighted with a sufficiently large factor. Since such an error is not Gaussian, we minimize a more general L^2 instead of a χ^2. The panels 5 and 16 of Fig. 7 show the examples of the best-fit model curves (red dashed curves). These curves are similar (typically within observational 1σ error bars) to the best-fit model curves from the likelihood maximization method mentioned above. The best-fit c-parameter values are plotted in the right panel of Fig. 8. This figure shows that all the best-fit c values are positive, and are

consistent with the values from the likelihood maximization method. Moreover, the best-fit values of c from fits with and without upper limits are consistent with each other for bursts 16 and 18 (right panel of Fig. 8).

Finally, we check if the change of persistent emission during a burst can qualitatively affect the fractional amplitude evolution. We calculate the amplitudes for all 0.25 s time bins of all 27 bursts (Table 1), as described in § 2.4. We find that, although the absolute values of fractional amplitudes are somewhat affected by f_a (the amplitude values typically change by 0.9 times the data error calculated considering f_a), their relative values for a burst are not largely affected. This means that the shapes of the fractional rms amplitude versus time curves do not qualitatively change when the effects of persistent emission evolution is considered. We give examples for two bursts in Fig. 9.

3.3. *Fractional amplitude evolution for sources other than 4U 1636–536*

We perform a similar analysis, as mentioned in § 3.2, for the 24 bursts with rise oscillations from nine neutron star LMXBs listed in Table 2. Oscillations during the rise were detected in 1 bin for 13 bursts, in 2 bins for 7 bursts and in 3 bins for 2 bursts and 4 bins for 2 bursts. Fig. 10 shows the fractional oscillation amplitude versus time curves for the rising phases of these bursts. These curves suggest that the amplitude decreases with time. Moreover the amplitude profiles appear to have concave shapes. To verify these, we fit the these curves with the ϕ-function of Eqn. 3. Since for each of these 24 bursts the number of time bins with detected rise oscillations is small, we can use only the weighted Least-square minimization method (see § 3.2) to find the best-fit parameter values. The best-fit c-parameter values cluster on the right of the $c = 0$ line (Fig. 11), implying that the fractional amplitude profiles are of concave shapes. Thus the results for these nine sources are similar to those for 4U 1636–536 (§ 3.2).

3.4. *Burst groups for 4U 1636–536*

As mentioned in § 1, Maurer & Watts (2008) reported that the burst rise morphology is affected by burning regime, ignition latitude and thermonuclear flame spreading. They divided the bursts from 4U 1636–536 into three groups based on their peak fluxes and rising light curves, and discussed in detail how burning regime and ignition latitude, and hence the flame spreading parameters, are different in different burst groups. If this interpretation is true and if flame spreading causes the evolution of burst rise oscillations, then some properties of such evolution should also be different in different burst groups. We plan to test this.

To begin with, we need to identify which of the 27 bursts with rise oscillations belongs to which group. Since Maurer & Watts (2008) did not mention which group a given burst belongs to, we calculate the peak flux and the burst rise morphology (i.e., $\mathcal{C}$-parameter; see § 2.3) for each of 27 bursts mentioned in Table 1. Following the definition of Maurer & Watts (2008), these bursts are categorized into three groups: Group 1 (burst peak flux $< 50 \times 10^{-9}$ erg s^{-1} cm^{-2}; $\mathcal{C} < 0$), Group 2 (burst peak flux $< 50 \times 10^{-9}$ erg s^{-1} cm^{-2}; $\mathcal{C} > 0$) and Group 3 (burst peak flux $> 50 \times 10^{-9}$ erg s^{-1} cm^{-2}). We find 4, 6 and 17 bursts belonging to Groups 1, 2 and 3 respectively. The mean rise times of bursts from Groups 1, 2 and 3 are 3.66 s, 2.75 s and 1.76 s respectively. We divide the bursts from only 4U 1636–536 in groups, because sufficient number of bursts with rise oscillations is not available for any of the other nine sources (Table 2).

Now we try to find out if the distribution of burst rise time bins with detected oscillations are different in different burst groups. In the upper panel of Fig. 12, for each burst group, we plot the fraction ($X_{\rm n,osc}$) of burst rise time bins (each 0.25 s) with detected oscillations versus time bin index. This fraction for a given bin index indicates the probability (among bursts with rise oscillations) of having detected oscillations, or the likely strength of oscillations for that bin index for a particular burst group. So overall this panel gives an idea about the typical and maximum durations of oscillations during burst rise for each group. More specifically, this panel indicates that oscillations can exist for at most $\sim$ 2.25 s for Group 1 bursts, $\sim$ 2.75 s for Group 2 bursts, and $\sim$ 1.25 s for Group 3 bursts, measured from the burst onset. The fraction ($X_{\rm n,osc}$) fluctuates substantially for Group 1, may be partially due to a small (4) number of available bursts (see the lower panel of Fig. 12). However, $X_{\rm n,osc}$ shows a weak but overall increasing trend, which indicates that the oscillation becomes stronger in the later part of burst rise for this group. For the Group 2, $X_{\rm n,osc}$ is zero in the first time bin (may be because of the lowest count rates among all bins of all groups), then sharply goes to a high value, and finally gradually decreases, indicating a gradual decrease of the oscillation strength. For the Group 3, $X_{\rm n,osc}$ slightly increases first from a non-zero value, and then relatively quickly decreases, indicating a quick decrease of the oscillation strength. The lower panel of Fig. 12 shows the available total number of burst rise time bins versus the time bin index. This panel essentially reveals typical and maximum durations of burst rise for each burst group.

The above mentioned maximum duration of oscillations for each burst group (i.e., $\sim$ 2.25 s, $\sim$ 2.75 s and $\sim$ 1.25 s; see Fig. 12) depends on (1) the burst rise durations of that group, and (2) the fraction of rise time the oscillations persist for the bursts of that group. In order to disentangle these two causes, and to find out what fraction of rise time the oscillations persist for, we normalize the rise time of each burst to 1, and then replot the upper panel of Fig. 12 in Fig. 13 in a way mentioned in the caption of Fig. 13. This figure shows that for Group 3, the oscillations persist at most 60% of the rise time, while for the other two groups, the oscillations can survive for the entire durations of burst rise for some bursts. Finally, we note that Figs. 12 and 13 show that the evolution of burst rise oscillations is different in different burst groups, as expected (see the first paragraph of this subsection).

4. DISCUSSION

In this paper, we investigate if the thermonuclear flame spreading gives rise to oscillations during the rising phases of bursts from several neutron star LMXBs, and if so, then what the implications of these oscillations are. In § 4.1, we discuss the roles of low fractional amplitude and low count rate for non-detection and intermittent detections of burst

rise oscillations. In § 4.2, we argue that the observed fractional amplitude evolution during burst rise is consistent with thermonuclear flame spreading, and the flame speed is possibly latitude-dependent. In § 4.3, we mention three remaining puzzles regarding the flame spreading origin of burst rise oscillations, and discuss them in the context of three burst groups proposed by Maurer & Watts (2008). Finally in § 4.4, we detail the implications of our results.

4.1. *Intermittent- and non-detection of burst oscillations*

One of the most puzzling aspects of burst rise oscillations is that it is not detected from most bursts, and even when it is found from a burst, it is usually detected intermittently and for a fraction of the rise time. A simple reason for this could be the low count rates or intensities (see § 1). In § 2.2, we show that the detection of the burst rise oscillations depends on two factors: the fractional rms amplitude and the count rate parameter. Fig. 3 clearly shows that the red-square detection points spread over a large range of count rate parameter values (see § 3.1) for the individual 0.25 s time bins. Moreover, these detection points do not cluster at the higher values of the count rate parameter. These mean that the low count rates cannot entirely explain the non-detections of oscillations, and low fractional amplitudes must also be a reason for such non-detections. Note that this conclusion remains valid, even when the change of persistent emission during bursts is considered (see Fig. 5). This is also supported by Fig. 4, which shows that the fraction of bursts with detection of oscillations overall decreases with the time bin index, even though the intensity (and hence the count rate parameter) is expected to increase with the bin index. However, as expected, intensity also affects the detection. This can be inferred from the increase and decrease of the ratio of Fig. 4 in a shorter time scale, as well as from Fig. 6 and the corresponding K-S test described in § 3.1.

4.2. *Fractional amplitude evolution and flame spreading*

Now the question is, if low fractional amplitudes are an important reason for non-detection and intermittent detections of oscillations, can burst rise oscillations originate from thermonuclear flame spreading? Before addressing this question (see § 4.3), we attempt to find out if the fractional amplitude evolution for 27 bursts from 4U 1636–536 (Table 1) and 24 bursts from the other nine sources (Table 2) support the flame spreading scenario. A visual examination of Fig. 7 and Fig. 10 clearly shows that the fractional amplitude evolution for each burst is consistent with decreasing with time. As mentioned in § 3.2, a quantitative measurement for the best case (burst 16 of 4U 1636–536) reveals that the amplitude decreases with time with a significance of $\approx 99.99\%$. Furthermore, the minimum count rate parameter value at which the oscillation is detected increases with the time bin index (Fig. 3; see also Fig. 5 for a weaker trend). From Eqn. 1, this implies that the fractional rms amplitude decreases with time. As discussed in § 1, such a decrease of fractional amplitude strongly suggests that the thermonuclear flame spreading gives rise to burst rise oscillations in these sources.

Figs. 8 and 11 show the best-fit c-parameter values of the empirical model given in Eqn. 3. All these values for 4U 1636–536 from three different methods (see § 3.2) clearly cluster on the positive side of the $c = 0$ line (Fig 8). Similarly, all the best-fit c values for nine other sources also cluster on the positive side of the $c = 0$ line (Fig 11). This strongly suggests that the fractional rms amplitude versus time curves are concave, i.e., at first the fractional amplitude decreases fast, and then it does not change much. Note that the same suggestion was made by Bhattacharyya & Strohmayer (2007b), but for only two bursts, that too without any quantification. Therefore, the current paper reports a significant progress, because it confirms the previous result with a much larger sample size (51 bursts from ten sources), and a quantification with an empirical model. Bhattacharyya & Strohmayer (2007b) numerically showed that a convex shape of a fractional amplitude versus time curve implies an isotropic flame spreading, while a concave shape could be a result of the latitude-dependent flame speed, likely due to the Coriolis force (see also § 1). Therefore, our detailed analysis tentatively reveals the possible effects of the Coriolis force on flame spreading, as expected for rapidly spinning neutron stars, such as the ten sources considered in this paper (Spitkovsky et al. 2002). Finally, we note that the change of persistent emission during a burst does not affect our conclusions (§ 3.2).

4.3. *Flame spreading in three burst groups*

Although the fractional amplitude evolution reported in § 3.2 and § 3.3 supports the flame spreading origin of burst rise oscillations, the following puzzles remain. (1) Why is the oscillation intermittently detected for a given burst? In the flame spreading scenario, if the fractional amplitude decreases monotonically, how can the oscillation be not detected in a former time bin, but be detected in a later time bin? (2) Why is the oscillation not detected, i.e., fractional amplitudes are quite low for most bursts? What kind of flame spreading process can explain this? (3) What determines the duration of detected oscillations during the rise of a given burst?

One may attempt to understand the puzzle 1 in the following ways. (a) The fractional amplitude may not always decrease monotonically. The increase of the burning area causes the decrease of amplitude, but the change of the polar angle of the burning region center (as the flames spread) may sometimes increase the fractional amplitude due to the viewing geometry (see more discussion later regarding the Group 1 bursts). So if the fractional amplitude increases by the net effect, the oscillation may be detected in a time bin after a non-detection in the previous bin. (b) Eqn. 1 implies that the detection of oscillations depends on fractional amplitude and burst intensity. Hence, if the intensity does not increase sufficiently as the amplitude decreases in a time bin, the oscillation may not be detected in that bin, but may be detected in a later bin with sufficiently higher intensity.

In order to address the puzzles 2 and 3, we need to discuss the burst oscillations together with various burst groups. As mentioned in § 3.4, the maximum duration of oscillations for each burst group depends on (1) the durations of burst rise in that group, and (2) the fractions of burst rise time with oscillations in that group. The former may be primarily determined by the time scale of flame spreading and fuel burning, while the latter may be deter-

mined by the fraction of rise time in which an azimuthal asymmetry caused by the burning region persists. After disentangling the above two causes (§ 3.4), we find that, for Group 3, the visible portion of the burning region becomes azimuthally symmetric much before the flame spreading is over. But for Groups 1 and 2, the burning region can remain somewhat azimuthally asymmetric till the end of the flame spreading. We now examine if these findings are consistent with the conclusions of Maurer & Watts (2008), and attempt to address the puzzles 2 and 3 mentioned above.

Maurer & Watts (2008) concluded that the Group 3 bursts are He bursts with equatorial ignition. The He burst interpretation is consistent with the shorter rise times of the Group 3 bursts (see the lower panel of Fig. 12; also mentioned by Maurer & Watts (2008)). According to Spitkovsky et al. (2002), an exactly equatorial ignition will make the burning region azimuthally symmetric very quickly, and hence no burst rise oscillation is expected. This may explain why rise oscillations are not detected for more than half (64%) of the bursts of Group 3 (Maurer & Watts 2008). If the ignition of some of the Group 3 bursts are off (but near) equatorial, then we expect initial oscillations, which may disappear soon. This is because, since the flame speeds at lower latitudes are more than those at higher latitudes (Spitkovsky et al. 2002), the azimuthal asymmetry of the burning region may disappear soon (much before the flame spreading is over) by spreading in the direction of latitudes. This is consistent with the above mentioned observation (Fig. 13) that the oscillations exist during a fraction ($\leq$ 60%) of the rise time. Note that a slightly off-equatorial ignition could happen because of an off-equatorial higher temperature (e.g., by random fluctuation or due to the effects of previous bursts).

According to Maurer & Watts (2008), the bursts of Groups 1 and 2 are mixed H/He bursts with off-equatorial H ignition. These authors further concluded that the Group 1 bursts are ignited near the north pole while the Group 2 bursts are ignited near the south pole, considering that the observer's line of sight passes through the northern hemisphere. The longer rise times of the bursts from Groups 1 and 2 (see the lower panel of Fig. 12; also mentioned by Maurer & Watts (2008)) are consistent with the mixed H/He burst interpretation.

But are our results consistent with the Group 2 bursts being ignited near the south pole? In case of such ignitions of the Group 2 bursts, we expect the azimuthal asymmetry of burning region (near the south pole) to survive for quite some time, because of the low flame speed near the pole (Spitkovsky et al. 2002). During this time, the northern burning front should propagate fast towards the equator, and become azimuthally symmetric. So the asymmetry at the southern front should be the origin of the oscillations. These expectations are supported by the observed rise oscillations with larger durations for Group 2 bursts (Fig. 13). However we note that for a near-south-pole ignition, the entire southern hemisphere should be ignited and the southern azimuthal asymmetry should disappear much before the northern burning front reaches the north pole. But we find that the burning region can remain somewhat azimuthally asymmetric till the end of the flame spreading for Group 2 bursts (see above; also Fig. 13). One possible explanation to this is that the northern burning front stalls at the equator, as suggested by Cavecchi et al. (2013). Another question is why rise oscillations are not detected for most (77%) of the bursts of Group 2 (Maurer & Watts 2008). We note that, if the ignition happens too close to the south pole, the southern azimuthal asymmetry (if formed) may be out of sight, and hence no oscillations will be observed.

Now we examine if our results are consistent with the Group 1 bursts being ignited near the north-pole. In case of such ignitions of the Group 1 bursts, the fractional amplitude is expected to be initially small because of the near-face-on viewing geometry, unless the the observer's line of sight is far from the stellar spin axis. As the burning region expands towards the equator, the fractional amplitude may decrease because of the increasing burning area, but may increase due to the changed viewing geometry (see above). The latter is because, as the center of the burning region moves towards the equator, a larger fraction of this region periodically goes out of the view, increasing the fractional amplitude. A competition between the above two effects might partially cause the fluctuations of the ratios $X_{\rm n,osc}$ and $X'_{\rm n,osc}$, as we find (see Figs. 12 and 13). Another question is why rise oscillations are not detected for most (93%) of the bursts of Group 1 (Maurer & Watts 2008). We note that, if the ignition happens too close to the north pole, a significant azimuthal asymmetry may not be formed (depending on the viewing geometry), and hence no oscillations will be observed.

Therefore, our findings based on the evolution of burst rise oscillation amplitude are broadly consistent with the conclusions of Maurer & Watts (2008) based on an independent method of burst rise morphology, if we consider the latitude-dependent flame speeds suggested by Spitkovsky et al. (2002). Such comparison provides a required sanity check and gives confidence to the flame spreading model of burst rise oscillations. Moreover, our study of the evolution of burst rise oscillations for various burst groups (§ 3.4) helps to probe the reasons of the absence of rise oscillations in most bursts (puzzle 2 mentioned above) and what determines the durations of burst rise oscillations (puzzle 3 mentioned above).

4.4. *Implications of results*

Now we briefly discuss the implications of our finding, that the burst rise oscillations are likely to be caused by the thermonuclear flame spreading possibly under the influence of the Coriolis force. As we discuss below, our finding will be very important (1) to probe the physics of thermonuclear bursts and flame spreading, and (2) to make the burst rise oscillation method (Bhattacharyya 2010) to measure the neutron star parameters more reliable.

(1) Even without going into the details, our finding implies that flames cover the entire surface of the neutron star in ~ 2.5 s. Note that, if the burst rise oscillation amplitude evolutions were not due to the flame spreading, then that might imply the flames covering the neutron star surface within the first time bin, i.e., in 0.25 s (see § 1). This may have important implications on the flame spreading conditions like viscosity. For example, for a near-polar ignition

on a typical neutron star of 10 km radius, if the flame spreads within 0.25 s to cover the stellar surface, a rough estimate gives a flame speed of ~ 120 km s^{-1}. On the other hand, a rough estimate of flame speed from a spreading time scale of 2.5 s is ~ 12 km s^{-1}. Now, as mentioned in § 1 and Spitkovsky et al. (2002), for a typical neutron star of mass 1.4 $M_\odot$, radius 10 km, spin frequency 582 Hz, and considering h and t_n to be 10 m and 0.1 s respectively, the values of the flame speed are ~ 6 km s^{-1} and ~ 160 km s^{-1} assuming a weak and a maximum turbulent viscosity respectively. Therefore, our results support a weak turbulent viscosity for flame spreading. More burst parameters can be constrained by future observations with the LAXPC instrument of *Astrosat* (Agrawal 2006), and more effectively with a next generation X-ray mission like *LOFT* (Del Monte et al. 2012; Mignani et al. 2012).

(2) If burst oscillations originate from one or two hot spots on the neutron star surface, then such oscillations can be used as a tool to measure mass and radius of neutron stars, and hence to constrain the stellar equation of state models (Bhattacharyya (2010); Lo et al. (2013); also § 1). Therefore, it is very important to verify if burst oscillations originate from hot spots, because constraining equation of state models is a fundamental problem of physics and an important science goal for future X-ray missions (e.g., *NICER*, *LOFT*; see Lo et al. (2013)). Our finding suggests that burst rise oscillations originate from a hot spot (albeit expanding due to flame spreading), and hence is important to make burst oscillations a more reliable tool.

5. SUMMARY

Here we summarize the key points of this paper.
(1) We study the evolution of fractional amplitude of burst rise oscillations for 51 bursts from ten neutron star LMXBs. Previously, this was reported only for a few bursts (see § 1).
(2) Our detection criterion of burst rise oscillations in 0.25 s time bins is quite stringent (3σ; § 2.2), considering the small numbers of total counts in such short time bins. This contributes to the reliability of our conclusions.
(3) With detailed simulations, we find that the contribution of the systematic error due to the non-constant intensity within a 0.25 s burst time bin to the total fractional amplitude error is less than 0.4% for our typical data count rates (see § 2.2).
(4) We study the roles of low fractional amplitude and low count rate for non-detection and intermittent detections of rise oscillations in many bursts.
(5) We find a decreasing trend of burst rise oscillation amplitude with time. This is consistent with thermonuclear flame spreading. To the best of our knowledge, we, for the first time, quantify this trend by fitting with empirical models and by doing F-tests (§ 3.2 and § 3.3). We find that the decrease of amplitude is 4σ significant for the best case (§ 3.2). Moreover, it is important to note that an opposite trend is not found from any of the 51 bursts.
(6) From our fits of the burst rise oscillation amplitude versus time, we find not only decreasing trends, but also concave-shaped profiles for all the 51 bursts (§ 3.2 and § 3.3; Figs. 8 and 11). This implies latitude-dependent flame speeds, possibly due to the effects of the Coriolis force (see § 1).
(7) We, for the first time, explore and find that the shapes of oscillation amplitude profiles with and without persistent emission variation during burst rise are consistent with each other (see § 3.2).
(8) Maurer & Watts (2008) reported that the burst rise morphology can be used to probe burning regime, ignition latitude and thermonuclear flame spreading (see § 1 and § 3.4). Our findings based on an independent method of the evolution of burst rise oscillation amplitude are broadly consistent with their interpretation (§ 4). This comparison provides a sanity check for our conclusions.
(9) Our findings suggest a weak turbulent viscosity scenario for flame spreading (§ 4).
(10) Our findings imply that burst rise oscillations originate from an expanding hot spot, thus making burst oscillations a more reliable tool to constrain the neutron star equation of state models (§ 4).

We thank an anonymous referee for constructive comments which improved the paper.

REFERENCES

Agrawal, P. C. 2006, Advances in Space Research, 38, 2989
Asai, K., Dotani, T., Nagase, F., & Mitsuda, K. 2000, ApJS, 131, 571
Bhattacharyya, S. 2007, MNRAS, 377, 198
Bhattacharyya, S. 2010, Advances in Space Research, 45, 949
Bhattacharyya, S., & Strohmayer, T. E. 2005, ApJ, 634, L157
Bhattacharyya, S., & Strohmayer, T. E. 2006a, ApJ, 636, L121
Bhattacharyya, S., & Strohmayer, T. E. 2006b, ApJ, 641, L53
Bhattacharyya, S., & Strohmayer, T. E. 2006c, ApJ, 642, L161
Bhattacharyya, S., & Strohmayer, T. E. 2007a, ApJ, 656, 414
Bhattacharyya, S., & Strohmayer, T. E. 2007b, ApJ, 666, L85
Bhattacharyya, S., Strohmayer, T. E., Miller, M. C., & Markwardt, C. B. 2005, ApJ, 619, 483
Cavecchi, Y., Watts, A. L., Braithwaite, J., & Levin, Y. 2013, MNRAS, 434, 3526
Chakraborty, M., & Bhattacharyya, S. 2012, MNRAS, 422, 2351
Chakrabarty, D., Morgan, E. H., Muno, M. P., Galloway, D. K., Wijnands, R., van der Klis, M., & Markwardt, C. B. 2003, Nature, 424, 42
Cumming, A., & Bildsten, L. 2000, ApJ, 544, 453
Del Monte, E., Donnarumma, I., & LOFT Consortium 2012, Mem. Soc. Astron. Italiana, 83, 352
Feigelson, E. D., & Babu, G. J. 2013, Planets, Stars and Stellar Systems. Volume 2: Astronomical Techniques, Software and Data, 445
Feigelson, E. D., & Nelson, P. I. 1985, ApJ, 293, 192
Fryxell, B. A., & Woosley, S. E. 1982, ApJ, 261, 332
Galloway, D. K., Muno, M. P., Hartman, J. M., Psaltis, D., & Chakrabarty, D. 2008, ApJS, 179, 360
Isobe, T., Feigelson, E. D., & Nelson, P. I. 1986, ApJ, 306, 490
Jahoda, K., Markwardt, C. B., Radeva, Y., et al. 2006, ApJS, 163, 401
Lamb, D. Q., & Lamb, F. K. 1978, ApJ, 220, 291
Lo, K.-H., Miller, M. C., Bhattacharyya, S., & Lamb, F. K. 2013, ApJ, 776, 19
Maurer, I., & Watts, A. L. 2008, MNRAS, 383, 387
Mignani, R. P., Zane, S., Walton, D., et al. 2012, IAU Symposium, 285, 372
Miller, M. C. 1999, ApJ, 515, L77
Miller, M. C., & Lamb, F. K. 1998, ApJ, 499, L37
Muno, M. P., Fox, D. W., Morgan, E. H., & Bildsten, L. 2000, ApJ, 542, 1016
Muno, M. P., Özel, F., & Chakrabarty, D. 2002, ApJ, 581, 550
Nath, N. R., Strohmayer, T. E., & Swank, J. H. 2002, ApJ, 564, 353
Spitkovsky, A., Levin, Y., & Ushomirsky, G. 2002, ApJ, 566, 1018

Strohmayer, T., & Bildsten, L. 2006, Compact stellar X-ray sources, 113
Strohmayer, T. E., & Markwardt, C. B. 1999, ApJ, 516, L81
Strohmayer, T. E., & Markwardt, C. B. 2002, ApJ, 577, 337
Strohmayer, T. E., Markwardt, C. B., Swank, J. H., & in't Zand, J. 2003, ApJ, 596, L67
Strohmayer, T. E., Zhang, W., & Swank, J. H. 1997, ApJ, 487, L77
Strohmayer, T. E., Zhang, W., Swank, J. H., White, N. E., & Lapidus, I. 1998, ApJ, 498, L135
Swank, J. H., Becker, R. H., Boldt, E. A., Holt, S. S., Pravdo, S. H., & Serlemitsos, P. J. 1977, ApJ, 212, L73
van Straaten, S., van der Klis, M., Kuulkers, E., & Méndez, M. 2001, ApJ, 551, 907
Watts, A. L. 2012, ARA&A, 50, 609
Watts, A. L., Strohmayer, T. E., & Markwardt, C. B. 2005, ApJ, 634, 547
Wolynetz, M. S. 1979a, Appl. Stat., 28, 185
Wolynetz, M. S. 1979b, Appl. Stat., 28, 195
Worpel, H., Galloway, D. K., & Price, D. J. 2013, ApJ, 772, 94

Table 1

Log table of 27 thermonuclear X-ray bursts with detected burst rise oscillations from the neutron star LMXB 4U 1636–536 (stellar spin frequency ≈ 582 Hz) observed with *RXTE* PCA (see § 2.1).

Burst ID[1]	Burst ID[2]	Date	Time[3]	ObsID
1	1	1996-Dec-28	22:39:24	10088-01-07-02
2	2	1996-Dec-28	23:54:04	10088-01-07-02
3	6	1998-Aug-19	11:44:39	30053-02-02-02
4	8	1998-Aug-20	05:14:12	30053-02-02-00
5	9	1999-Feb-27	08:47:29	40028-01-02-00
6	13	1999-Jun-18	23:43:04	40028-01-08-00
7	15	1999-Jun-21	19:05:53	40031-01-01-06
8	16	1999-Sep-25	20:40:49	40028-01-10-00
9	24	2000-Oct-03	23:32:48	40028-01-20-00
10	25	2000-Nov-05	04:21:59	50030-02-01-00
11	26	2000-Nov-12	18:02:28	50030-02-02-00
12	31	2001-Apr-30	05:28:34	50030-02-10-00
13	37	2001-Aug-23	00:50:33	60032-01-04-04
14	45	2001-Sep-30	14:47:17	60032-01-12-00
15	61	2002-Jan-09	00:26:38	60032-01-20-00
16	75	2002-Jan-12	21:35:34	60032-05-03-00
17	77	2002-Jan-13	01:29:03	60032-05-03-00
18	84	2002-Jan-14	01:22:36	60032-05-05-00
19	102	2002-Jan-22	07:07:20	60032-05-10-00
20	109	2002-Jan-30	23:06:55	60032-05-12-00
21	110	2002-Feb-05	22:21:51	60032-05-13-00
22	111	2002-Feb-11	17:35:07	60032-05-14-00
23	115	2002-Apr-26	05:07:18	60032-05-18-00
24	127	2005-Mar-23	05:27:58	91024-01-10-00
25	138	2005-Jun-11	02:42:04	91024-01-50-01
26	148	2005-Aug-10	05:36:36	91024-01-80-00
27	150	2005-Aug-16	01:45:36	91024-01-83-00

[1] Burst ID used in this paper.
[2] Corresponding burst indices from Galloway et al. (2008).
[3] Start time of burst in UT.

TABLE 2

LOG TABLE OF 24 THERMONUCLEAR X-RAY BURSTS WITH DETECTED BURST RISE OSCILLATIONS FROM NINE NEUTRON STAR LMXBS OBSERVED WITH *RXTE* PCA (SEE § 2.1).

Source name	Frequency (Hz)[1]	Burst ID[2]	Burst ID[3]	Date	Time[4]	ObsID
4U 1608–52	620	1	8	1998 Apr 11	06:35:31	30062-01-02-05
		2	10	2000 Mar 11	01:42:36	50052-01-04-00
		3	21	2002 Sep 7	02:26:15	70059-01-20-00
		4	22	2002 Sep 9	03:50:29	70059-01-21-00
MXB 1659–298	567	1	2	1999 Apr 9	14:47:34	40050-04-01-00
4U 1702–429	329	1	4	1997 Jul 26	14:04:18	20084-02-02-00
		2	8	1999 Feb 22	04:56:05	40025-04-01-01
		3	9	2000 Jun 22	11:57:46	50030-01-01-04
		4	15	2001 Apr 1	15:47:17	50030-01-11-00
		5	24	2004 Feb 29	06:32:16	80033-01-04-02
		6	26	2004 Mar 1	23:26:40	80033-01-05-01
4U 1728–34	363	1	14	1997 Sep 19	12:32:58	20083-01-01-01
		2	15	1997 Sep 20	10:08:52	20083-01-01-02
		3	16	1997 Sep 21	15:45:31	20083-01-02-01
		4	17	1997 Sep 21	18:11:07	20083-01-02-01
		5	64	1999 Aug 19	09:33:48	40019-03-02-00
		6	68	1999 Aug 20	05:54:45	40019-03-03-00
		7	96	2001 Oct 27	23:53:44	50030-03-09-01
KS 1731–260	524	1	7	1999 Feb 23	03:09:01	40409-01-01-00
		2	8	1999 Feb 26	17:13:09	30061-01-04-00
1A 1744–361	530	1	1	2005 Jul 16	22:39:56	91050-05-01-00
SAX J1750.8–2900	601	1	2	2001 Apr 12	14:20:31	60035-01-02-02
4U 1916–053	270	1	9	1998 Aug 1	18:23:49	30066-01-03-03
Aql X–1	549	1	24	2001 Jul 1	14:18:37	60054-02-02-01

[1] Spin frequency of the sources in Hz.
[2] Burst ID used in this paper.
[3] Corresponding indices from Galloway et al. (2008).
[4] Start time of burst in UT.

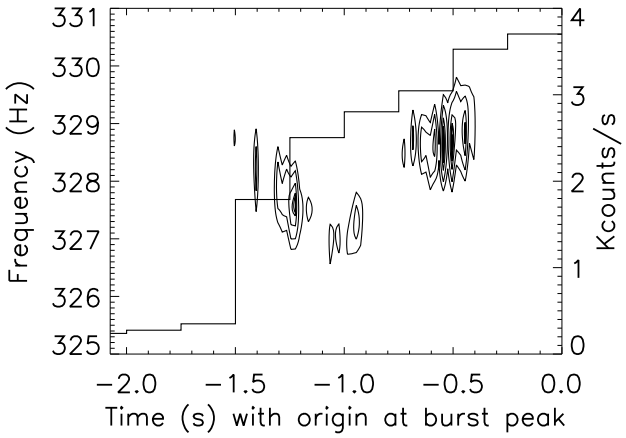

FIG. 1.— Power contours of oscillations in the frequency-time space during the rising phase of burst 6 (Table 2) from 4U 1702-429. The power contours show that the frequency of oscillations changes apparently erratically, and oscillations are present for short intervals during the rise. The histogram exhibits the burst intensity with time. This figure explains why phase-timing analysis technique cannot be used to estimate the frequency−time profile for the rising phase of many bursts (see § 2.2).

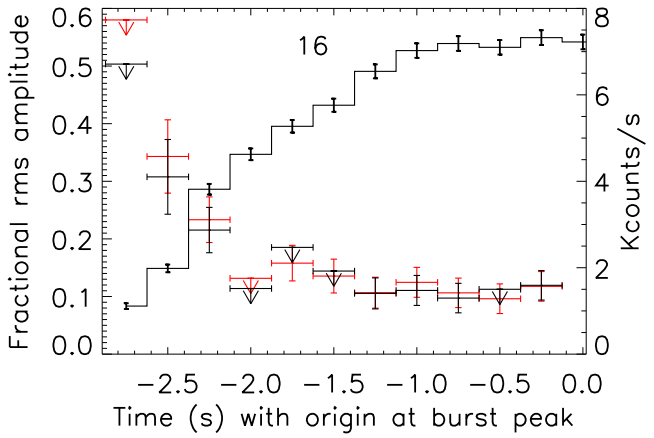

FIG. 2.— Fractional rms amplitude evolution (red and black points with error bars) of burst rise oscillations, and burst rise light curve (histogram) for the *RXTE* PCA burst 16 from 4U 1636–536 (Table 1). For the red points, the oscillation frequencies are estimated using our method (§ 2.2), while for the black points, the oscillation frequencies are estimated using the phase-timing analysis technique (Muno et al. 2000). This figure shows that fractional rms amplitude versus time curves from the two techniques are consistent with each other (§ 2.2).

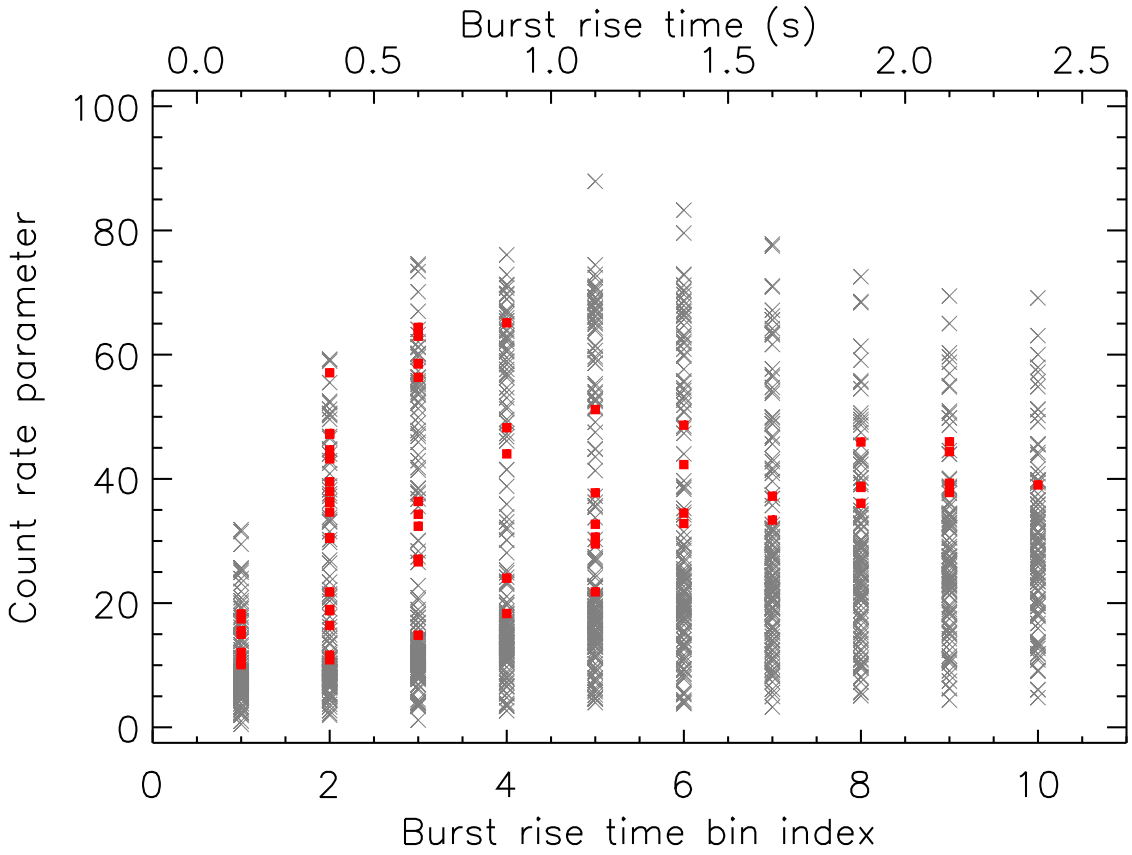

FIG. 3.— Count rate parameter [$= (N_{\rm T} - N_{\rm Per})/N^{\rm err}$] of thermonuclear bursts versus time bin (each of 0.25 s) index during burst rise (see § 2.2). Here $N_{\rm T}$ is the total count rate, $N_{\rm Per}$ is the average background count rate and $N^{\rm err}$is the 1σ error. A total number of 161 bursts from 4U 1636–536 observed with *RXTE* PCA are used in this plot (see § 2). A grey cross corresponds to a time bin of a burst. The small red squares correspond to the cases where burst oscillation is detected. The distribution of red squares on the grey crosses clearly shows that the non-detections of burst oscillations are not solely due to low observed count rates (see § 3.1).

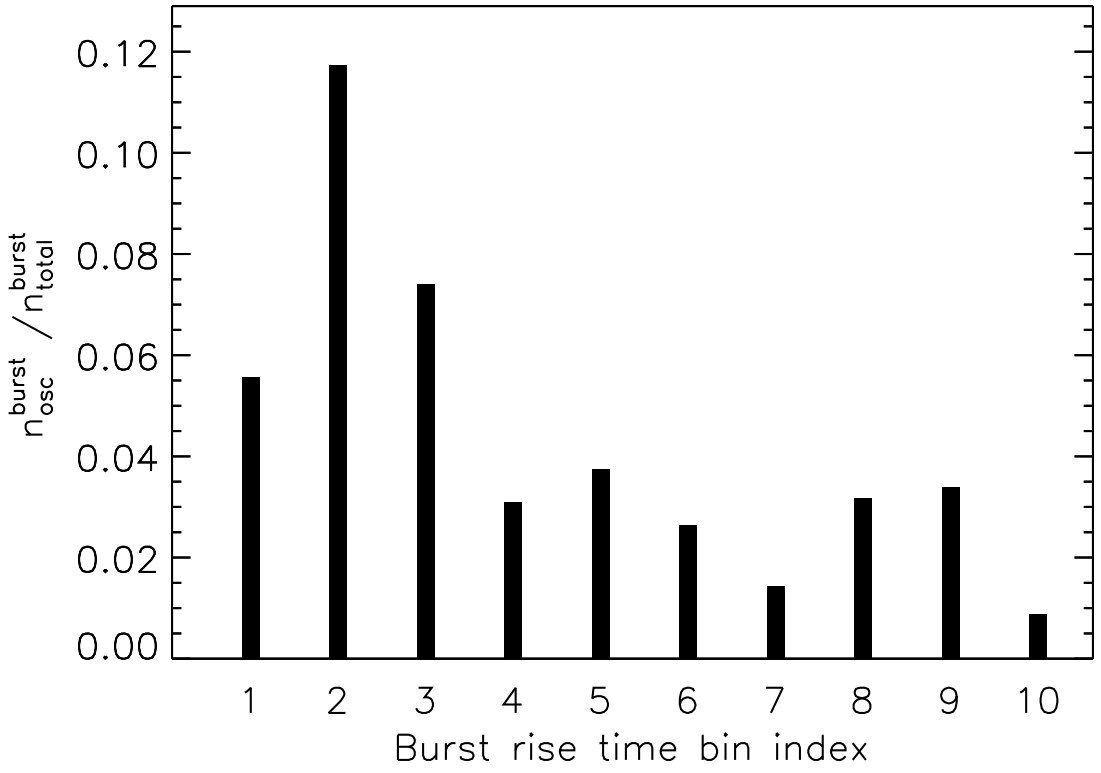

FIG. 4.— The fraction of thermonuclear bursts with detected burst rise oscillations versus time bin (each of 0.25 s) index during burst rise (see § 2). A total number of 161 bursts from 4U 1636–536 observed with *RXTE* PCA are used in this plot. For a given time bin, $n_{\rm osc}^{\rm burst}$ is the number of bursts with detected oscillations, and $n_{\rm total}^{\rm burst}$ is the total number of bursts. This figure shows that the fraction of bursts with detected oscillations overall decreases with time, although the burst intensity is expected to increase with time during burst rise (see § 3.1).

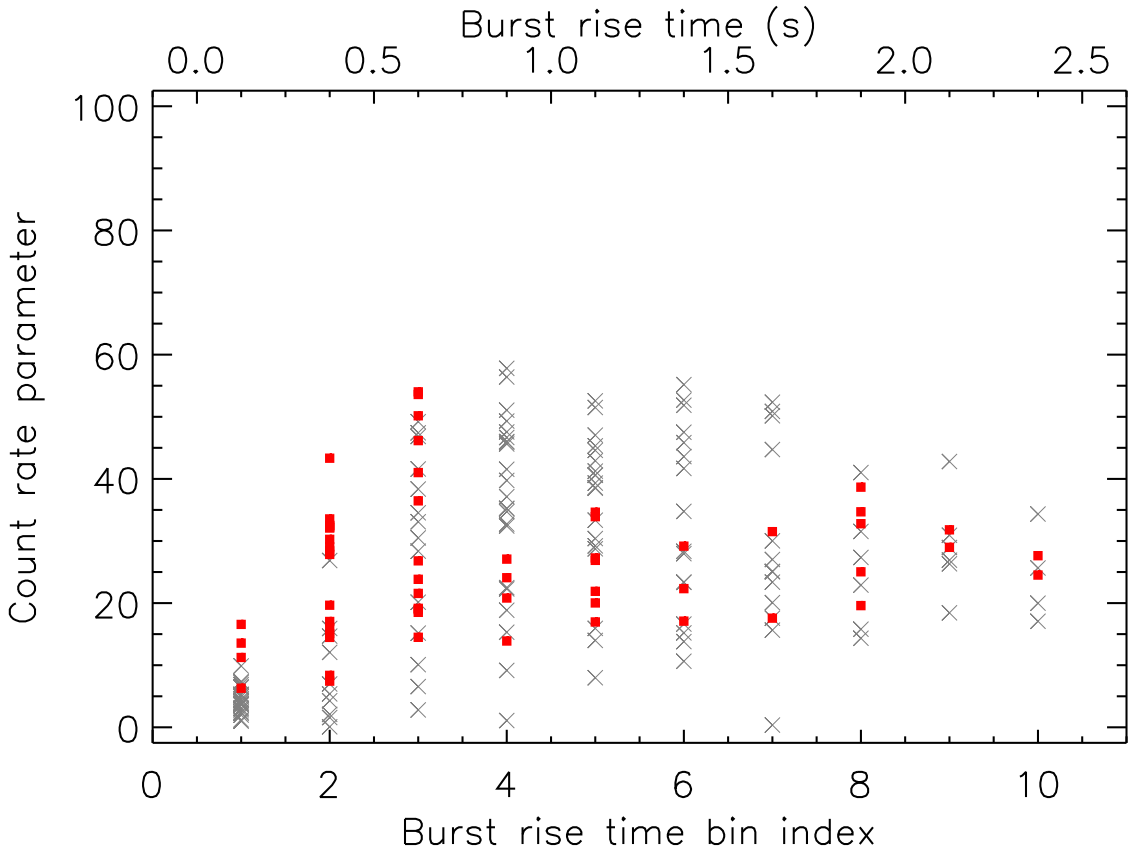

FIG. 5.— Similar to Fig. 3, but (a) including the effects of the changing persistent emission, i.e., considering f_a as described in § 2.4; and (b) for only the 27 bursts with oscillations detected in at least one time bin (see § 2 and § 3.1). This figure shows that the non-detections of burst oscillations are not solely due to low observed count rates, even when the effect of the changing persistent emission is considered.

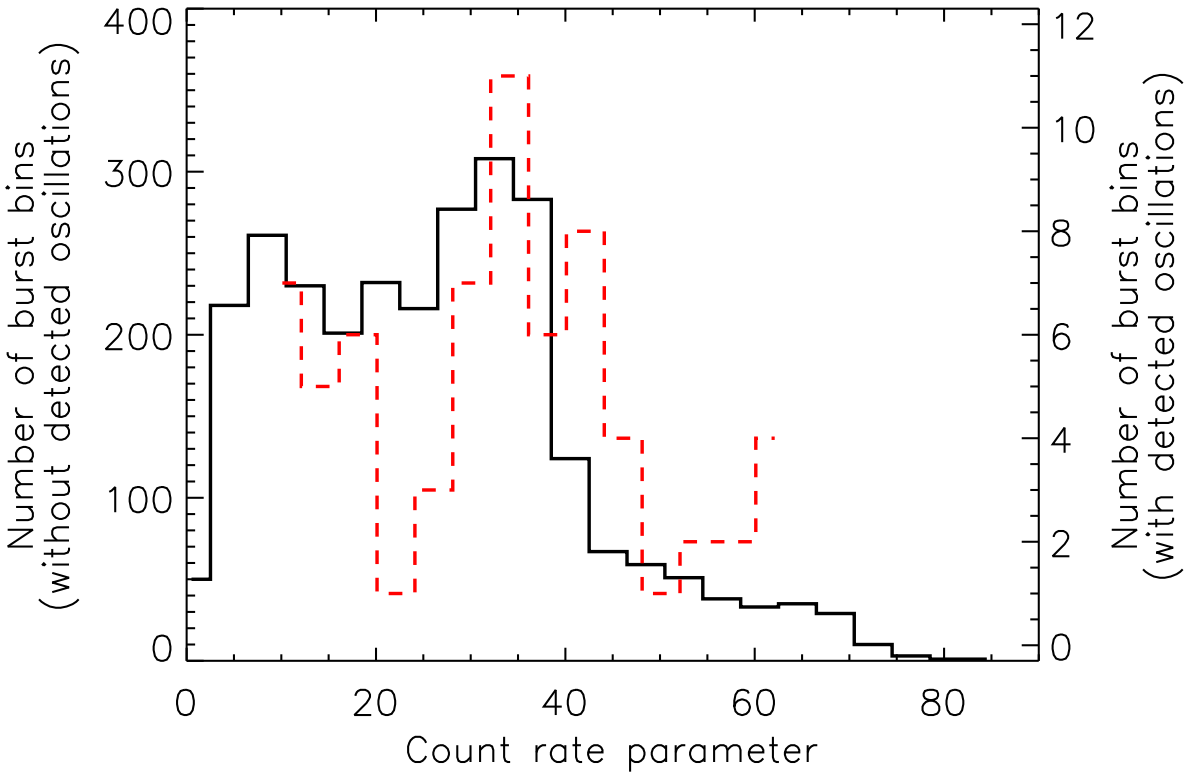

FIG. 6.— The distributions of 0.25 s rise time bins of all the 161 *RXTE* PCA bursts from 4U 1636–536 over the count rate parameter values in the following two cases: (1) bins without detected oscillations (solid black histogram; left y-axis), and (2) bins with detected oscillations (broken red histogram; right y-axis) (see § 3.1). From this figure, it appears that the second distribution is somewhat shifted towards the higher values of the count rate parameter relative to the first distribution, and hence the detection of oscillations somewhat depends on the burst intensity (§ 3.1).

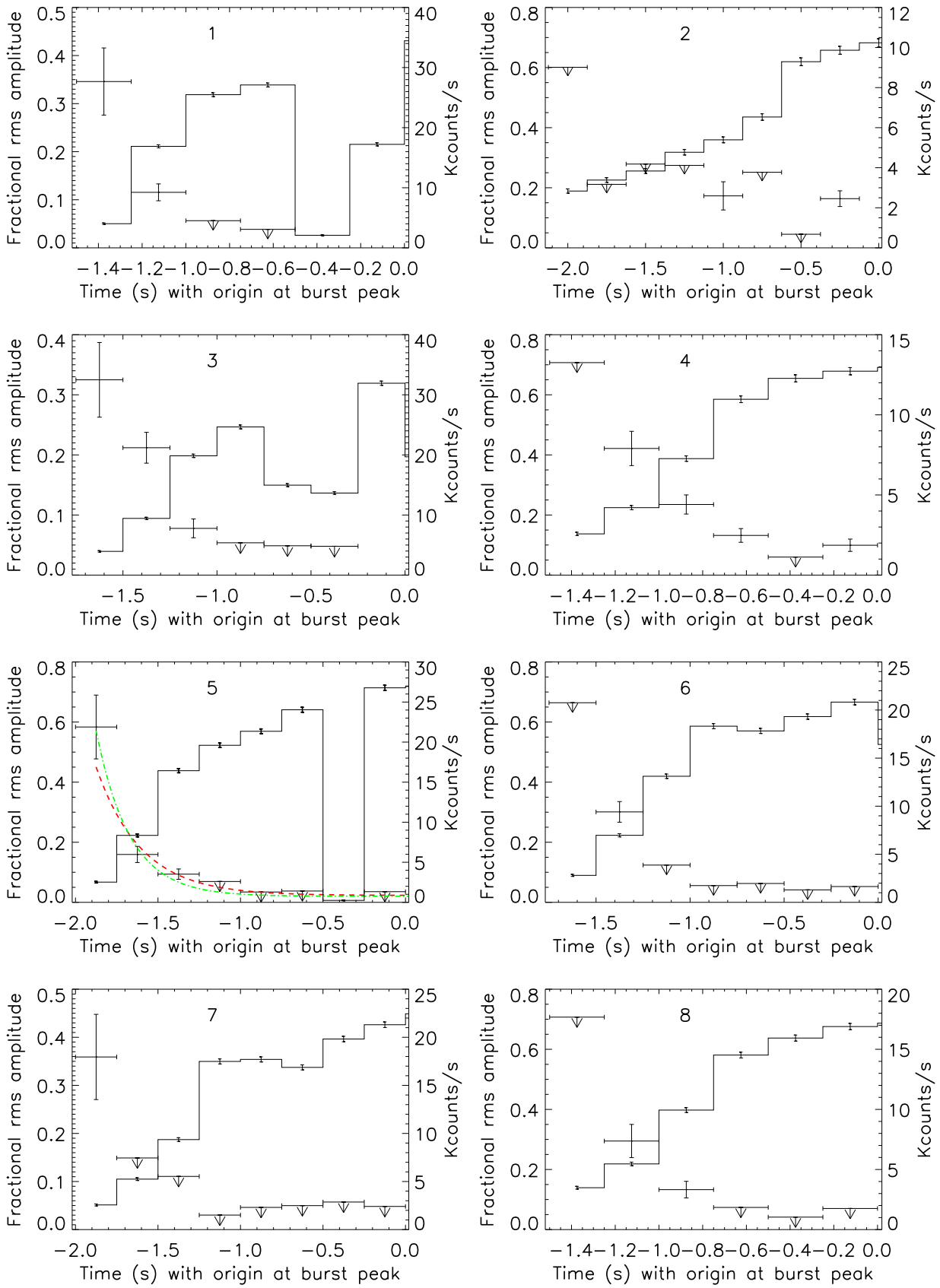

FIG. 7.— Time evolution of fractional rms oscillation amplitude (left-hand y-axis) and PCA count rate (histogram; right-hand y-axis) of thermonuclear bursts during rise. Each of 27 panels is for a burst from 4U 1636–536 with rise oscillations detected with *RXTE* PCA (see § 2.2). The y-error bars give the 1σ errors and the horizontal bars show the time bin size of 0.25 s. If oscillation is not detected (see § 2.2 for the criterion), an upper limit, denoted by an arrow, is given. A panel number gives the burst index quoted in the first column of Table 1. Model fits to the fractional rms amplitude evolutions are also shown for two representative bursts with small (burst no. 5) and large (Burst no. 16) number of time bins with detected oscillations. The red dashed curves and the green dash-dot curves show the best-fit empirical model $a - bc(1 - e^{-t/c})$ (t: time variable, a, b, c: parameters) for the weighted least square minimization method and the likelihood maximization technique respectively (see § 3.2). This figure shows that the fractional rms oscillation amplitude usually decreases with time during burst rise (§ 3.2).

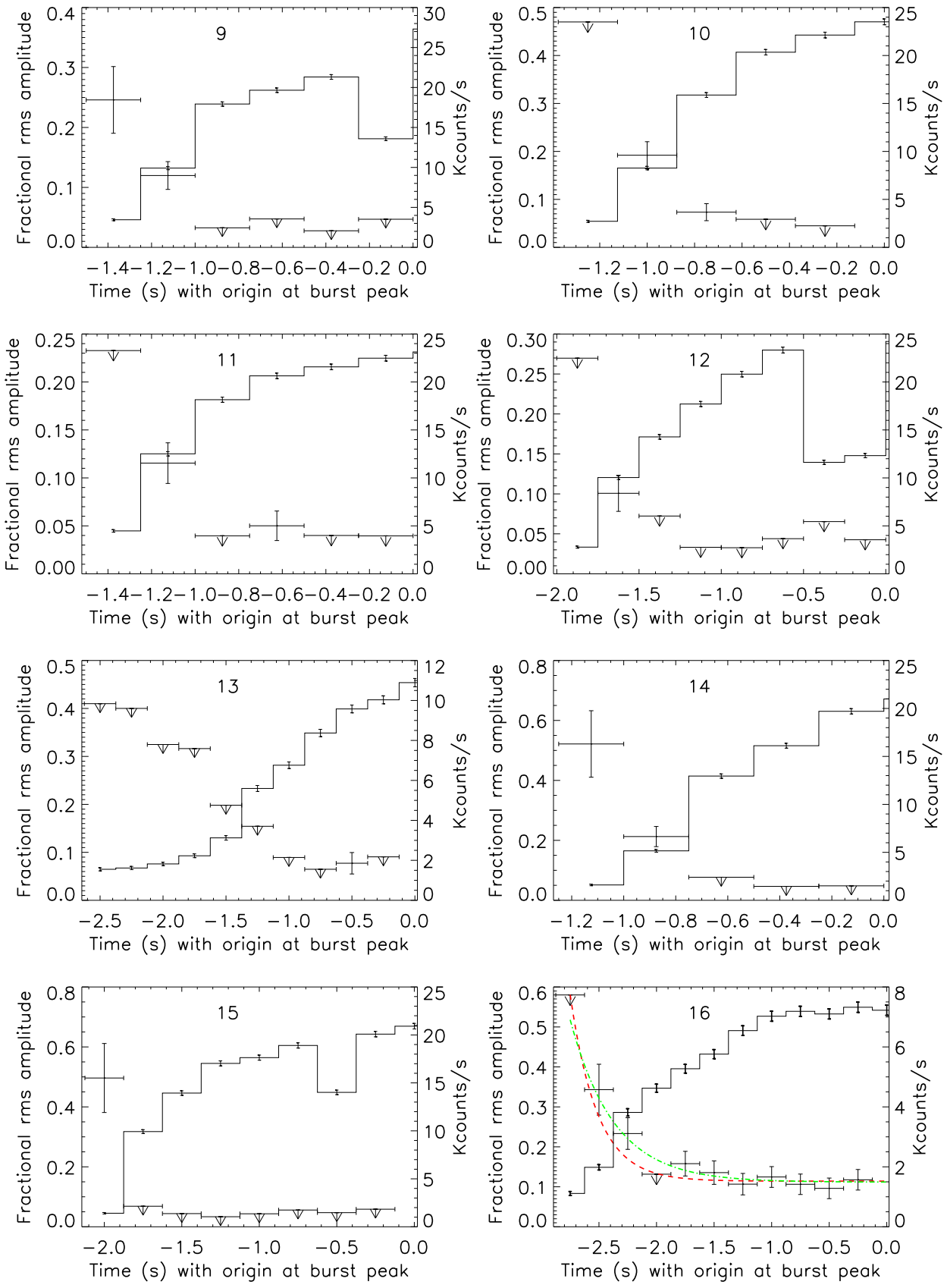

FIG. 7.— Continued.

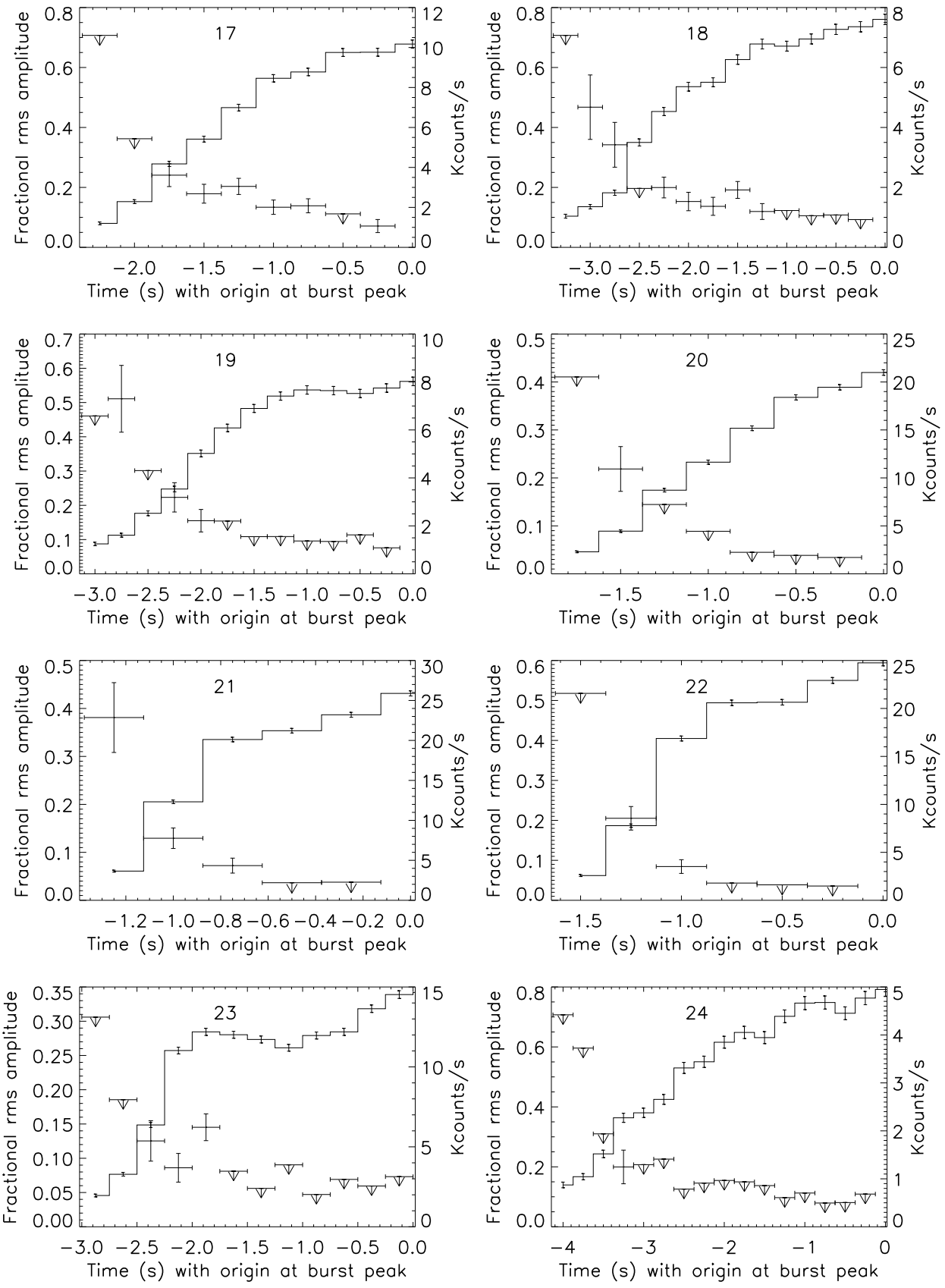

FIG. 7.— Continued.

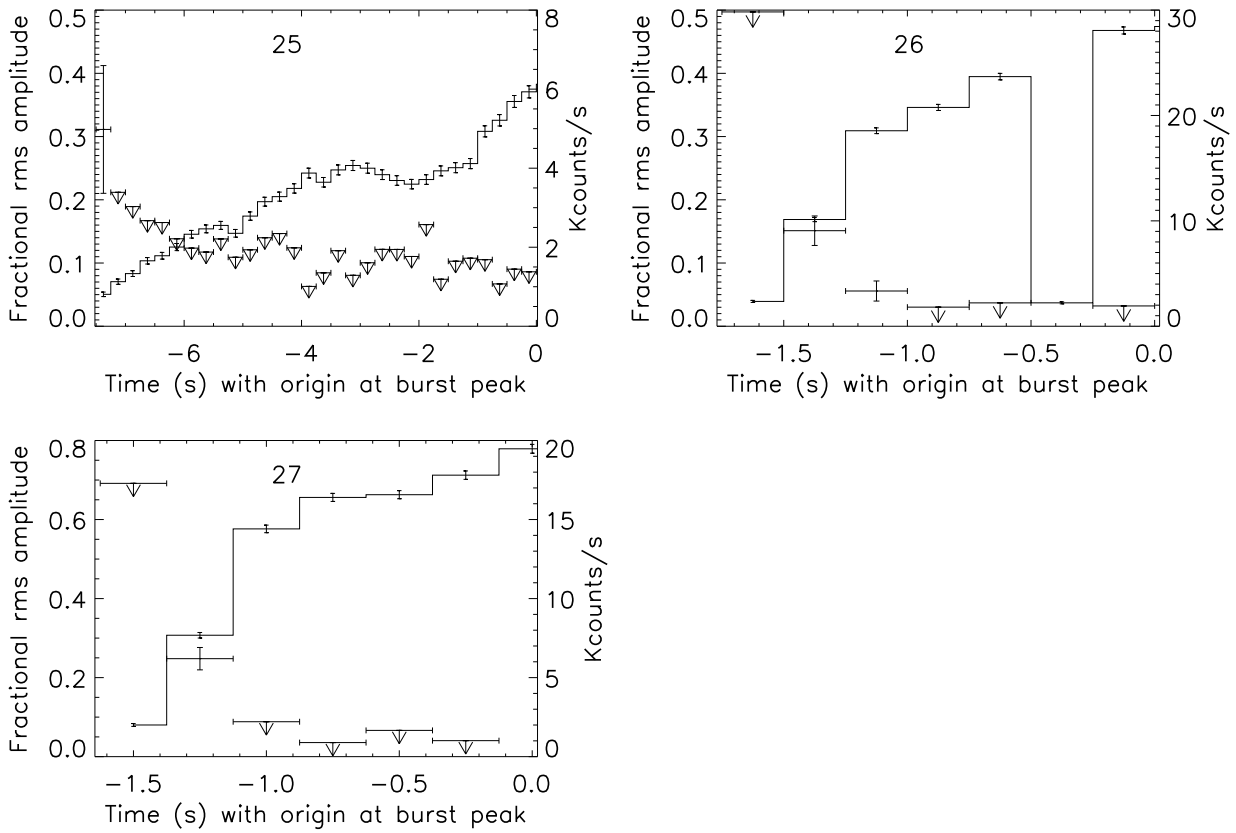

FIG. 7.— Continued.

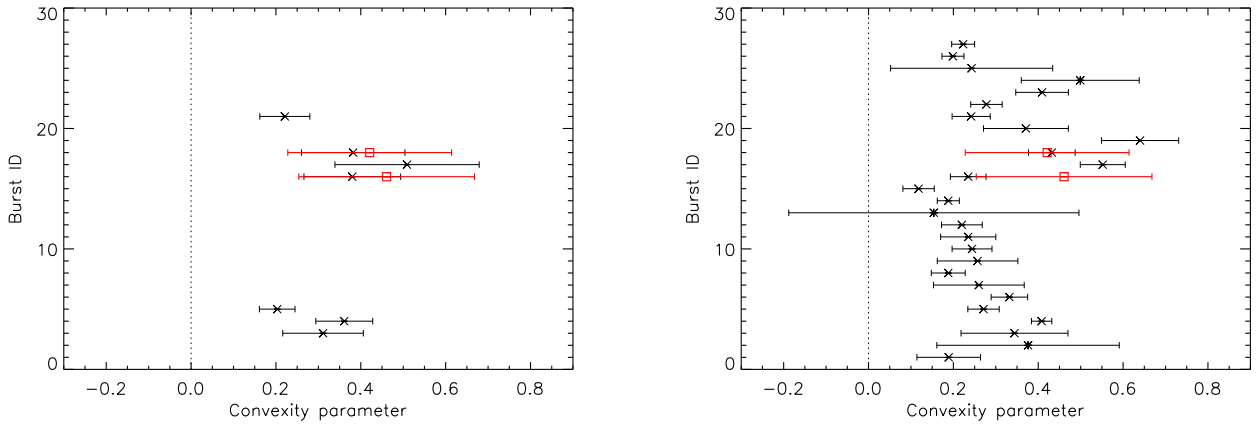

FIG. 8.— *Left panel*: the best-fit convexity parameter c (with 1σ error) for 4U 1636–536 bursts having oscillations during rise detected with *RXTE* PCA (see § 2.2; Table 1). The parameter c appears in the model $a - bc(1 - e^{-t/c})$, which is used to fit the time evolution of the fractional rms amplitude (see § 3.2). The black crosses are for fitting (including the upper limit points) using the likelihood maximization technique (see § 3.2). The red squares are for fitting excluding the upper limit points for two bursts (16 and 18) with detected oscillations in minimum five time bins, including at least one of the first two bins (see § 3.2). The dotted vertical line corresponds to $c = 0$. *Right panel*: similar to the left panel, but the black crosses and stars are for fitting (including the upper limit points) using the weighted least square minimization method, where the stars are for bursts with no detected oscillations in the first three time bins (see § 3.2). This figure shows that all the best-fit values of c cluster to the right of the dotted vertical line, implying latitude-dependent flame speeds, possibly due to the effects of the Coriolis force on thermonuclear flame spreading (see § 4).

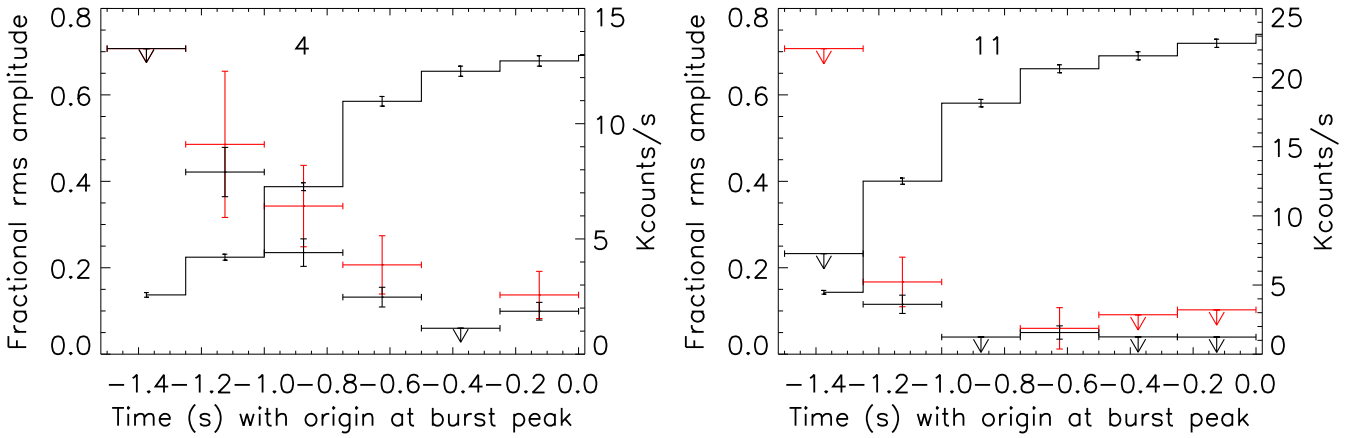

FIG. 9.— Similar to panels 4 and 11 of Fig. 7, but in addition to the points without considering f_a (shown in black), the points considering f_a are also shown (in red). This figure shows that the fractional rms oscillation amplitude usually decreases with time during burst rise, even when the effect of the changing persistent emission is considered (§ 3.2).

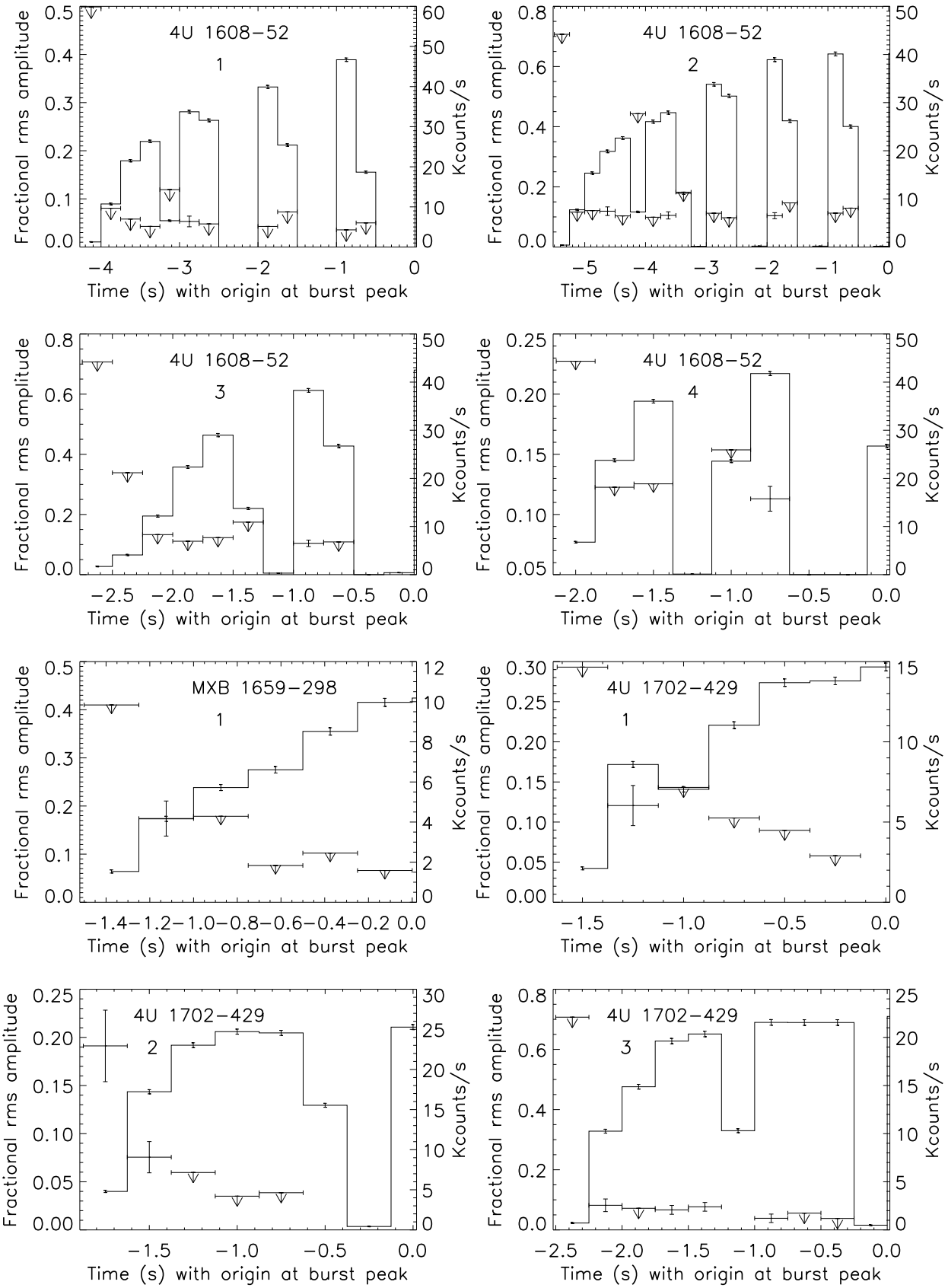

FIG. 10.— Same as Fig. 7, but for 24 bursts with rise oscillations from nine sources (mentioned in Table 2). Some bursts from some sources, especially 4U 1608–52, have a number of data gaps because of high intensity. These data gaps are excluded for the fractional rms amplitude calculation when possible (§ 3.3).

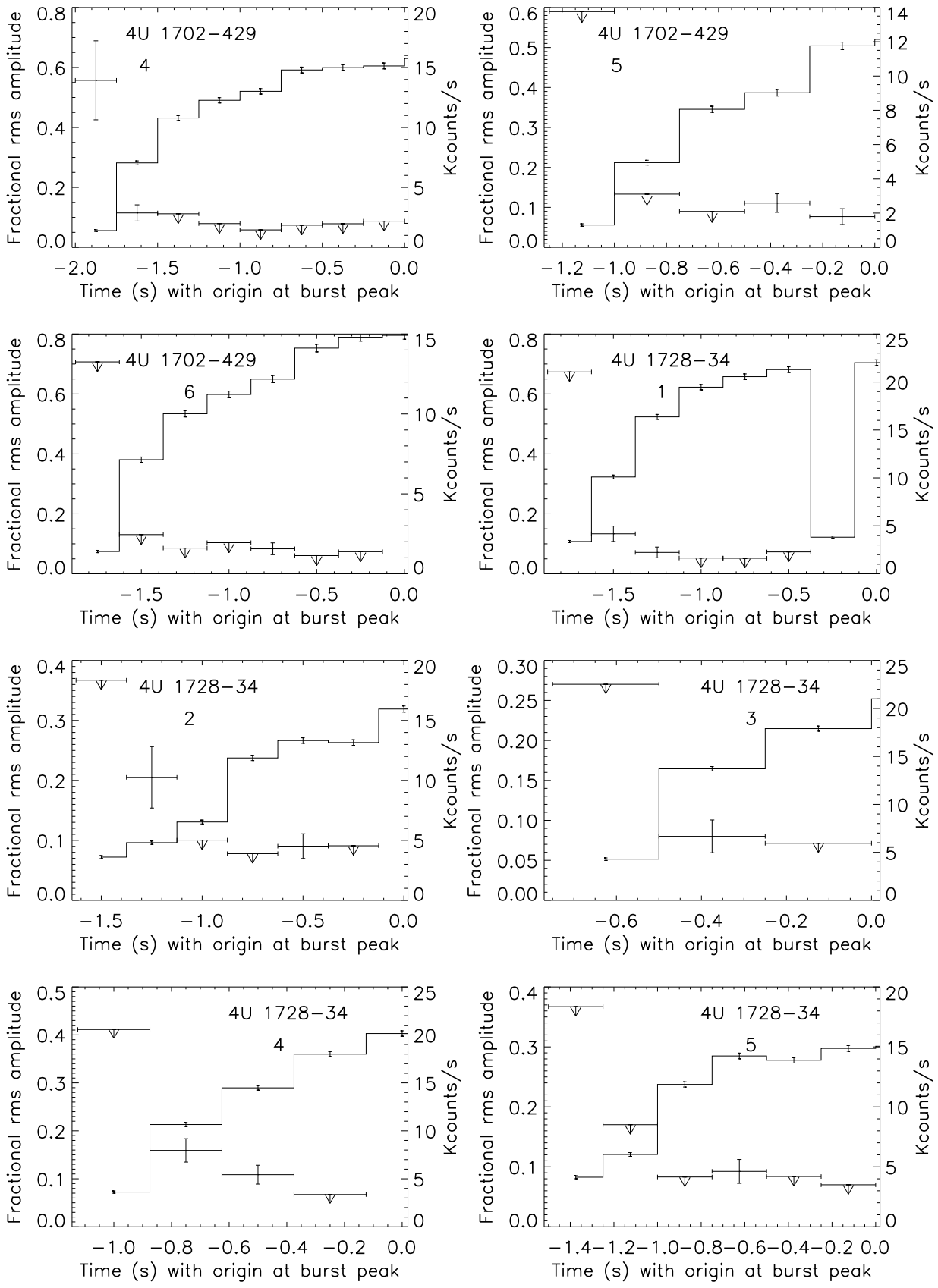

FIG. 10.— Continued.

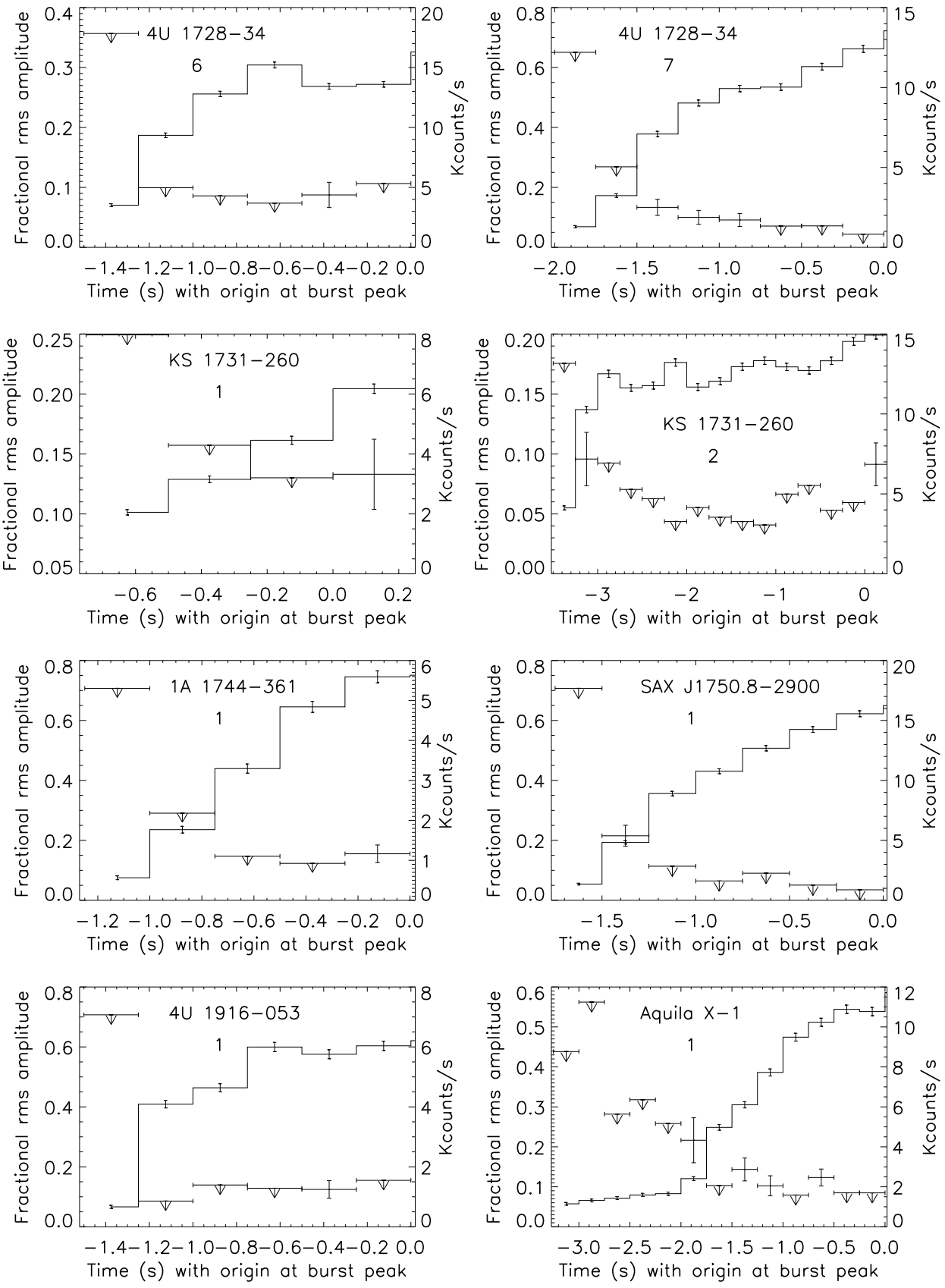

FIG. 10.— Continued.

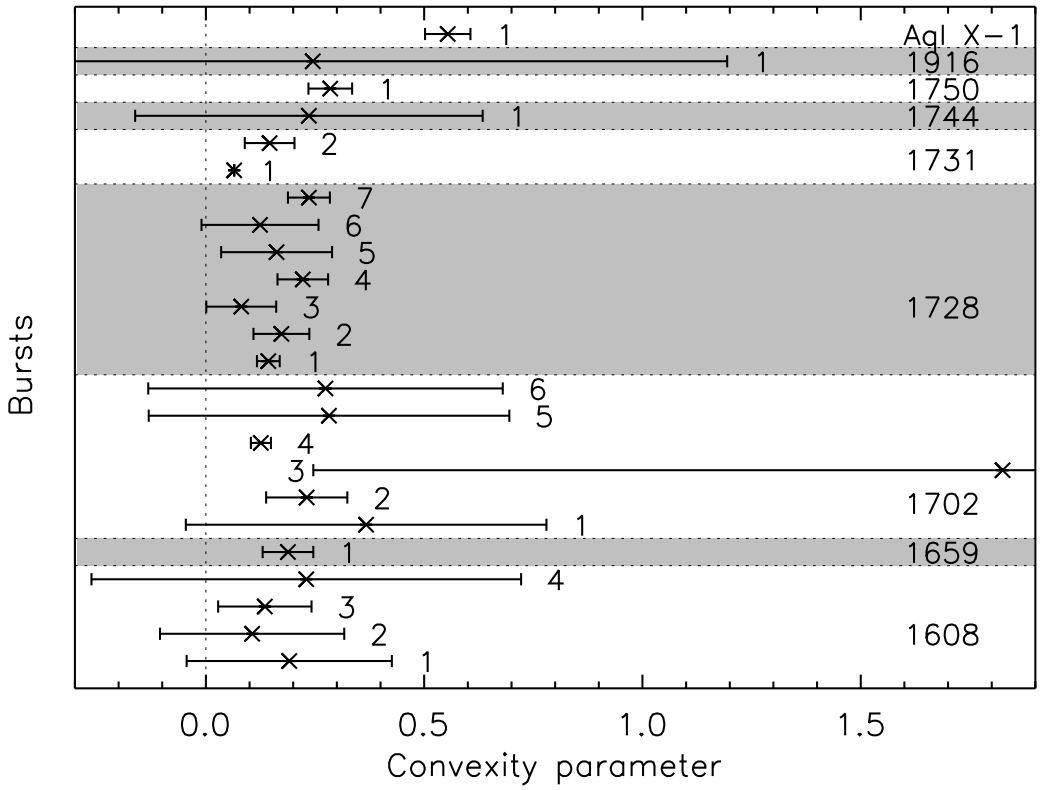

FIG. 11.— Similar to the right panel of Fig. 8, but for 24 bursts with rise oscillations from nine sources (mentioned in Table 2). In this case the y-axis represents the bursts from different sources (see Table 2 for source names and the corresponding burst numbers). The dotted horizontal lines separate the bursts from different sources (§ 3.3).

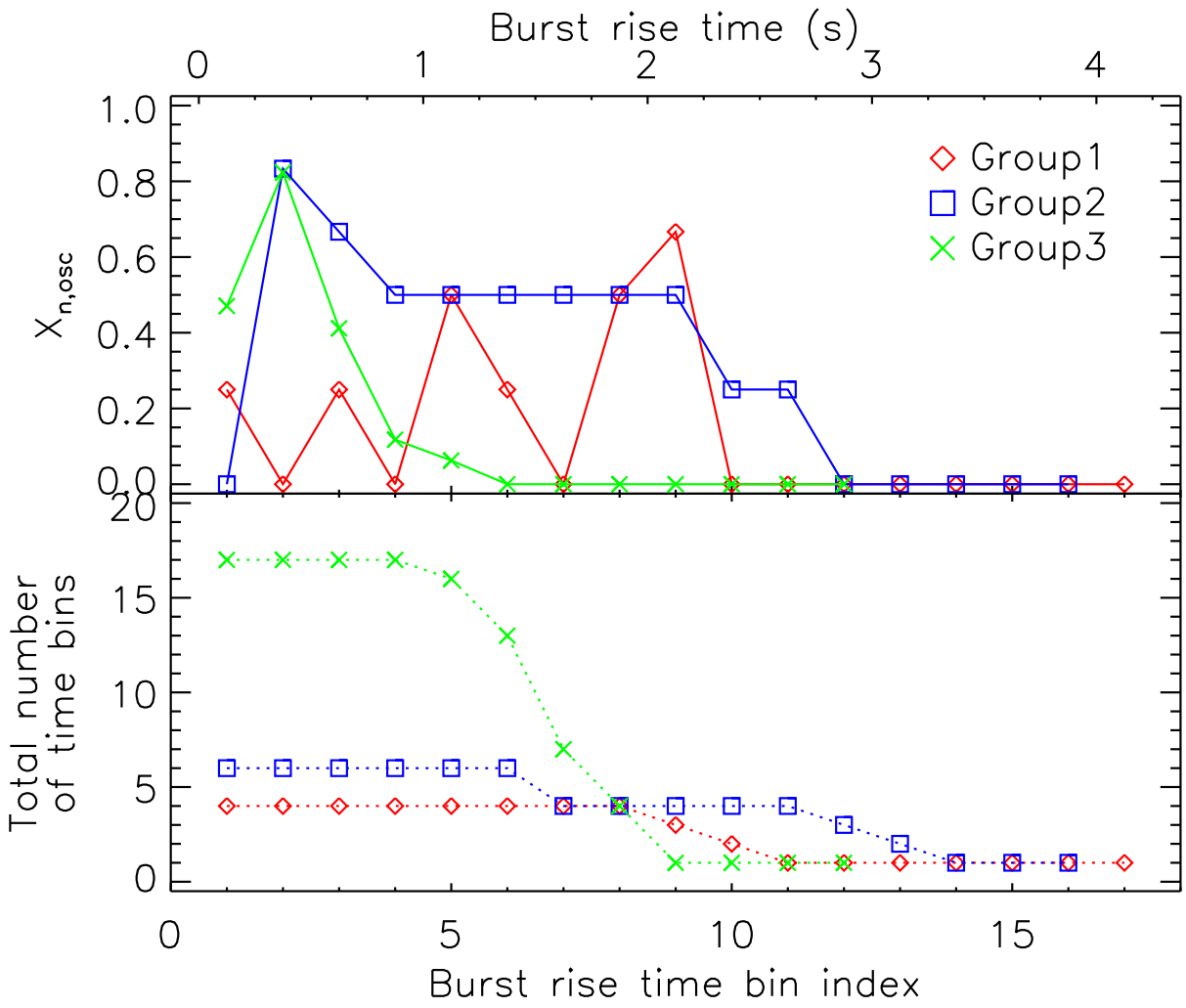

FIG. 12.— *Top panel*: fraction ($X_{\rm n,osc}$) of thermonuclear burst rise time bins (each 0.25 s) with detected oscillations versus time bin index for each morphological group as discussed in § 3.4. *Bottom panel*: for each morphological group, this panel shows the total number of burst rise time bins available for a given time bin index. In this figure, 27 4U 1636–536 bursts with oscillations during rise detected with *RXTE* PCA are considered (see § 2.2). This figure shows that rise times of Group 3 bursts are usually shorter than those of Group 1 and 2 bursts. Moreover, burst rise oscillations for Group 3 disappear typically much faster than those for other two groups (see § 3.4 and § 4).

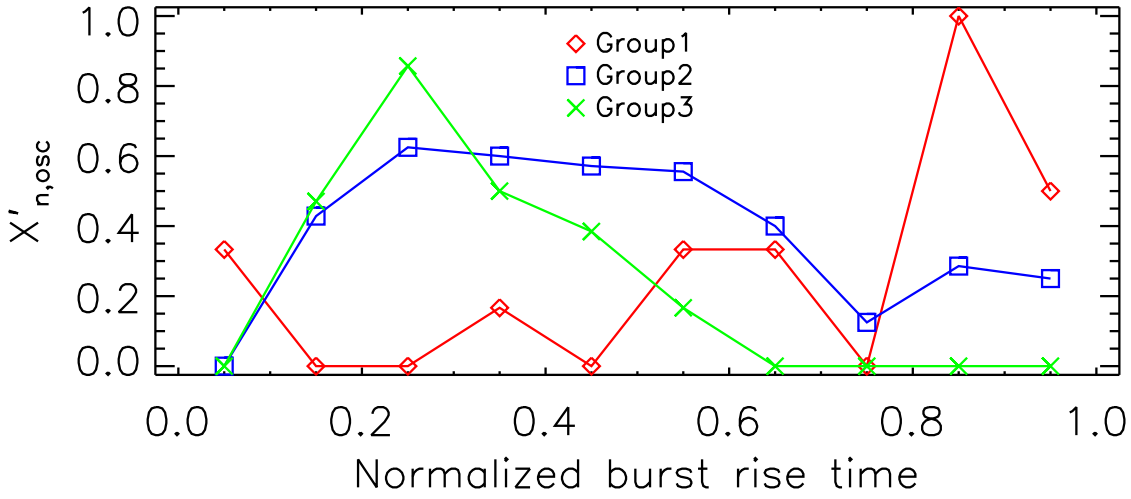

FIG. 13.— Similar to the upper panel of Fig. 12, but the x-axis is normalized as follows. The rise time of each burst is normalized to 1, and subsequently divided into 10 equal bins. Then considering all the bursts for a morphological group, the fraction ($X'_{\rm n,osc}$) of the $n^{\rm th}$ bins with detected burst rise oscillations is calculated ($n = 1, 2, ..., 10$). Finally, $X'_{\rm n,osc}$ is plotted with the normalized burst rise time (defined in the range $0 - 1$), which is calculated from n. This figure shows that typically oscillations last for a shorter fraction of burst rise for Group 3 than for other two groups (see § 3.4 and § 4).